Numerical study of passive flow control on the cooling of a matrix of surface-mounted cubes using LES

FRANZISKA SPEHR

Division of Fluid Dynamics

CHALMERS UNIVERSITY OF TECHNOLOGY

Göteborg, Sweden, 2007

Numerical study of passive flow control on the cooling of a
matrix of surface-mounted cubes using LES
FRANZISKA SPEHR

Division of Fluid Dynamics
Departement of Applied Mechanics
Chalmers University of Technology
SE-412 96 Göteborg
Sweden

Numerical study of passive flow control on the cooling of a matrix of surface-mounted cubes using LES

by

Franziska Spehr

FranziskaSpehr@gmx.de

Division of Fluid Dynamics

Department of Applied Mechanics

Chalmers University of Technology

SE-412 96 Göteborg

Sweden

Abstract

The main focus of the study was to investigate the influence of attaching vortex generators to the surface of floor mounted cubes on the heat transfer. The flow and heat transfer around a matrix of these cubes was performed by large-eddy simulation, LES. The numerical simulations were made for a fully developed turbulent flow over one cube mounted in the middle of a matrix of surface-mounted cibes. There was a constant heat flux generated equally from each cube of the matrix. Due to the periodicity of the flow, periodic boundary conditions were applied in both, the streamwise and the spanwise directions.

In order to study the influence of vortex generators on the flow structures and heat transfer coefficient, the flow and the convective heat transfer equations were solved around three different cubes configurations: a smooth cube, a cube with vortex generator 1 and a cube with vortex generator 2.

The vortex generators used in this investigation were a simple rib (vortex generator 1) and five small cubes (vortex generator 2) attached to the top and each of the side faces of the cube close to the streamwise edges. The flow Reynolds number based on the bulk velocity and the height of the channel was 13000 and the Reynolds number based on the bulk velocity and the height of the cube was 3860.

The standard Smagorinsky subgrid-scale model was used to model the unresolved scales and heat fluxes. The dependency of the meshes on the results was investigated by performing two computations with meshes having different numbers of nodes in case of the cube with vortex generator 2.

The LES results were compared with the experimental results and good agreement was found. Numerical flow visualization was used to provide a better insight into the flow structures and the heat transfer coefficient around the cubes. The LES results showed that the flow in the boundary layer around the cube with vortex generators was more turbulent and unsteady than the flow around the smooth cube without vortex generators. More turbulent structures were generated close to the surface of the cube resulting in a good mixing of the heat and hence high heat transfer coefficient arises.

Acknowledgments

This work was conducted at the Division of Fluid Dynamics at Chalmers University of Technology.

First of all I would like to express my sincere gratitude to my supervisor Hassan Hemida for all the help he gave to me. He has always had time for my questions and his very good and clear explaining was aiding in great much. Hassan taught me how to use the different computer programs and how to write this thesis. He enhanced my knowledge about fluid dynamics and heat transfer a lot.

I am very thankful that Professor Lars Darvidson was my examiner. He was made it possible for me to find a project and a supervisor in the Division of Fluid Dynamics at Chalmers. Lars helped me with my project by positive and encouraging advices for my work and also for the presentation of the thesis.

I also want to thank Prof. Herbert Oertel and Dr. Ulrich Dohrmann, who gave me the opportunity to do this project abroad.

Thank you to the whole Division of Fluid Dynamics!

Nomenclature

Upper-case Roman

A	area
C_p	specific heat at constant pressure
C_S	Smagorinsky model coefficients
$\mathcal{F}_j$	flux component
E	energy
Gr	Grashof number
Gr_H	Grashof number based on the height of the cube, H
H	height of the cube
K	kinetic energy $K = \frac{1}{2}\overline{u_i' u_i'}$
$\mathcal{L}$	integral length scale
M	Mach number
Pr	Prandtl number
Pr_{air}	Prandtl number of air, 0.71 (at 294 K)
Q	state vector in equations on conservative form
Q_{ij}	residual stresses
$\dot{Q}$	heat flow per unit time
Re	Reynolds number
Re_H	Reynolds number based on the height of the cube, H
R	gas constant
S_{ij}	strain rate tensor
T	temperature
T_{bi}	bulk temperature of the incoming flow, 294 K
$\overline{U_i}$	filtered velocity component
U_i'	subgrid-scale velocity component

Lower-case Roman

a	speed of sound
c_p	specific heat
g	acceleration due to gravity
h	heat transfer coefficient

h_j	subgrid heat fluxes
k	thermal conductivity constant
l	integral length scale
l	size of a body
$\dot{m}$	mass flow rate
p	pressure
$\overline{p}$	mean pressure
p'	fluctuating part of the pressure
t	time
u	fluid velocity
u	axial velocity component
u_0	upstream velocity
u_i	Cartesian components of velocity vector
u_b	bulk velocity of the incoming flow, 3.86 m/s
$\overline{u}$	mean velocity
u'	fluctuating part of the velocity
u_*	friction velocity
v	radial velocity component
v	velocity scale
v_K	Kolmogorov micro-scale of velocity
w	tangential velocity component
x_i	Cartesian coordinate vector component
y^+	non-dimensional resolution in the wall normal direction

Upper-case Greek

Δt	time step
Δ	filter width
Δ	size of one cell
$\Delta X_{Separation}$	length of the separation bubble
Δy_{down}	height of the stagnation line

Lower-case Greek

α_{SGS}	subgrid scale eddy diffusivity
β	volumetric thermal expansion coefficient
δ_{ij}	Kronecker's delta
ϵ	rate of dissipation of turbulent kinetic energy
ϵ	specific emissivity
η	length scale
η_K	Kolmogorov micro-scale of length
κ	specific heat ratio

μ	dynamic viscosity
μ_t	dynamic eddy viscosity
ν	kinematic viscosity ($\nu = \mu/\rho$)
ν_{SGS}	Smagorinsky eddy viscosity
ρ	density
ρ_{air}	density of air, 1.16 kg/m^3
σ	Stefan-Boltzmann constant, $\sigma = 5.67 \cdot 10^{-8} \frac{W}{m^2 K^4}$
σ_T	standard deviation of the temperature
τ	time scale
τ_K	Kolmogorov micro-scale of time
τ_{ij}	subgrid scale stress tensor
τ_W	wall-shear stress

Abbreviations

CFD	Computational Fluid Dynamics
DNS	Direct Numerical Simulation
FVM	Finite Volumes Method
LES	Large Eddy Simulation
RANS	Reynolds Averaged Navier-Stokes
SGS	Subgrid Scale
TDMA	Tridiagonal Matrix Algorithm
VG	Vortex Generator
VG1	a simple rib as Vortex Generator
VG2	small cubes as Vortex Generator

x

List of Figures

Contents

Chapter 1

Introduction

When electronic components are attached to a printed circuit, they, under concentrated heat dissipation conditions, act as a strong source of heat which might cause local overheating. It is generally believed that local overheating of integrated circuits (IC) is the major cause for the technical failure of electronic equipment. Hence, finding a way for an efficient heat removal from these components is crucial to ensure steady reliable long-term operations.

The production and development of a new generation of power-electronic components is controlled by the efficient design to remove the heat generated by these components.

In general the heat removal from an integrated circuit depends very much on the flow structures around it. The electronic component is a bluff body that produces flow with separations. The flow around an integrated electronic circuit can be approximated to be similar to the flow around a cube mounted on a surface.

Previous investigations of the flow around a surface-mounted cube found that different kinds of flow instabilities give rise to different flow structures around the cube.

At low and moderate Reynolds numbers, the flow separates from the side of the cube to form separation bubbles. The flow inside these bubbles circulates and it might be raped in its place if the bubbles are steady. The shear layers between these separation bubbles and the exterior fluid are highly turbulent and this gives rise to the so-called Kelvin-Helmholtz flow instability. This flow instability is responsible for shedding of vortex tubes in a regular fashion to the wake flow behind the cube, distortion of large scale vortices, production of small scales and eventually transition from laminar to turbulent flow. There is also flow instability in the wake flow behind the cube which is associated with the shedding of large scale vortices from the recirculation region to the far wake flow.

This flow instability is controlled by the flow Reynolds number and hence the high frequency mode in the shear layers between the recirculation region and the exterior fluid. The dominated shear layers around the cube make the flow structures very complicated.

Different numerical methods have been used in the past to study the flow around a single cube mounted on a surface. Krajnović and Davidson [1] and [3] used large-eddy simulation to investigate the flow structures around a surface-mounted cube in a fully developed channel flow. They used different techniques to visualize the flow. In their simulation, the Reynolds number was 40000 based on the incoming mean bulk velocity and the cube height. They found that the flow separates from the surface of the cube on the lateral and the top side faces of the cube. They visualized a horse-shoe vortex attached to the mounting surface, as shown in figure 1.1.
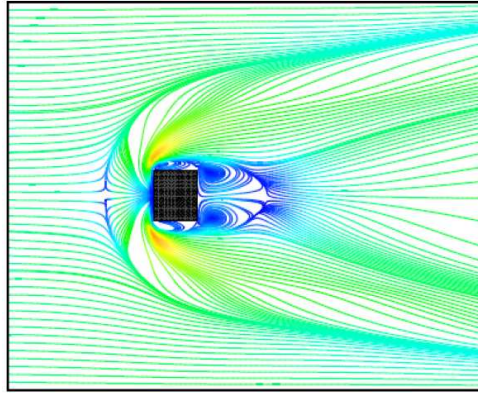
Figure 1.1: Streamlines of the mean flow projected onto the channel floor, Krajnović and Davidson [1]

Cone-like vortices are formed on the top-side face. These complex-flow structures are obtained using different flow simulations. The results are in a good agreement with the experimental results of Martinuzzi and Tropea [4], having done measurements in a low-speed wind tunnel. Yakhot et al. [5] studied the same cube at the relative low Reynolds number of 1870, based on the incoming bulk velocity and the cube height, using Direct Numerical Simulation (DNS) and they got similar flow structures.

The local heat transfer around such a wall mounted cube was also subject of some studies. Nakamura [6] experimentally discovered the heat transfer of a cube oriented 45° to flow direction to be lower than of a cube oriented perpendicular to the flow at the range of Reynolds numbers $4.2 \cdot 10^3 - 3.3 \cdot 10^4$.

The turbulent flow around multiple cubes is even more complicated. The wake structures from one cube interact with the structures of the other cubes and the mounting surface. The flow is characterized by the complex interior topology which induces the flow to separate and recirculate locally between the mounting surface and the cubes. The shedding of the large scale structures in the wake flow depends mainly on the flow Reynolds number and on the separation distance between the cubes. The flow structures, however, are highly unsteady and three-dimensional.

At present, there are remarkably few studies on local heat transfer around multiple three-dimensional objects. Meinders and Hanjalić [2] experimentally investigated the influence of the relative obstacle position on the convective heat transfer from a configuration of two wall-mounted cubes located in a fully developed turbulent channel. They found that the crucial parameter that influences the flow pattern and, consequently, the heat transfer is the longitudinal spacing between the cubes. Meinders and Hanjalić [7] also investigated experimentally a matrix of equidistant cubes mounted on one of the walls of a plane channel. Their investigation provided reference data on flow and heat transfer relevant to electronics circuitry. The investigations were done on an internally heated cube that was placed in the middle of the matrix of identical but non-heated cubes; all mounted on a constant temperature channel wall (See [7] and [8]). The surrounding cubes on the matrix ensured a fully developed flow with periodic boundary conditions. Due to the well-known boundary condition and its computational simplicity, their case and data are considered the bases for many of computational fluid dynamic simulations to get insight into the physics of the flow structures and heat transfer. Cheng et al. [9] and Zhong and Tucker [10] used the experimental data of Meinders and Hanjalić [7] to compare different simulation techniques (large-eddy simulation (LES), standard $k - \epsilon$ Reynolds-Averaged Navier-Stokes (RANS) and $k - l$ based hybrid LES/RANS). RANS simulation for flow with large scale unsteadiness was found not to perform as well as hybrid LES/RANS. LES calculations reproduced the complex features of the fully developed flow better than RANS calculations, but the associated computational cost and time were much bigger.

Despite that many attempts have been done in the past to understand the physics of the flow around single or multiple cubes very few attempts were performed to find a way to enhance the heat transfer from the cubes.

In this study, we investigate the influence of altering the turbulent boundary layer on the surfaces of the cubes on the enhancement of

3

heat transfer. This is done by generating small vortices on the surface of the cube using different vortex generators. The vortex generators in the present work are a simple rib and small dices mounted on the top and the side faces of the cubes. The Reynolds number of the flow is 13000, based on the incoming bulk velocity and height of the channel. The objective of the present work is to employ LES to investigate the influence of the vortex generators on the flow structures and the local heat transfer coefficient.

1.1   Vortex Generator

A vortex generator (VG) is a small device that influences the flow around a body. It creates small vortices and affects the flow separation. Vortex generators are used to delay the flow separation to control the boundary layer and to decrease the drag coefficient of vehicles (see [11] and figure 1.2 (a)). Very often VGs are used in aircraft at the wing as shown in figure 1.2 (b) to increase the lift coefficient by having less flow separation and therefor less air resistance. VGs can also be found in gas turbines to reduce the pressure drop. Another application of vortex

(a) VG at a cars back side [12]   (b) VG at the wing of an airplane [13]

Figure 1.2: Examples for vortex generators

generators is to enhance the heat transfer of a cooling surface. Here it is highly desired to have turbulent boundary layers that imply high mixing of the fluid particles. This could be arranged by the small scale vortices produced by the vortex generators, and in fact leads to a better convective heat transfer than without vortex generators. For this purpose the vortex generators should be tiny bluff bodies attached to the

cooling surface at the position where separation of the flow would start without them.

In case of multiple cubes behind each other, vortex generators could also change the size of the recirculation region in the wake of one cube and therewith it could change the incoming flow for the next cube.

Chapter 2

Turbulence

2.1   Introduction to Turbulence

Turbulence is the natural state for many flows. It differs from laminar flow in the way that its attributes like velocity or pressure are fluctuating in both, time and space. There is no precise and unique definition of turbulence, but one can see turbulent flow as a tangle of vortices.

The turbulent motions are often generated in the flow as a result of the three-dimensional flow instabilities. These instabilities are concentrated near the solid boundaries and behind bluff bodies. That is why the turbulent flow starts first in the boundary layer and then spreads to the external flow. That could be seen by studying transitional flow over a flat plate for instance. In case of bluff bodies, the flow instabilities and hence the transition to turbulence depends on the size of the body l, the velocity of the fluid u_0 and the kind of the fluid, which is described for example by the kinematic viscosity ν. These properties can be combined together to obtain the Reynolds number Re:

$$Re = \frac{u_o\, l}{\nu}. \tag{2.1}$$

By increasing the Reynolds number, the flow behind the body becomes more and more likely a turbulent flow. Figure 2.1 shows the flow structures around a circular cylinder at different Reynolds numbers. At very low Reynolds numbers, the flow is laminar everywhere and the flow instability, due to the existence of the cylinder, is too small to generate turbulent flow (see figure 2.1 (a)).

By increasing the Reynolds number, an adverse pressure gradient arises at the surface of the cylinder. Due to this adverse pressure gradient, the flow is likely to separate from the surface of the cylinder. The separation happens, if the inertia of the flow, the convective part in the

Navier-Stokes equation (2.9), is not high enough to overtake the adverse pressure gradient. Owing to the flow separation, the flow instability is strong enough to initiate turbulence in the wake (see figure 2.1 (b)). At that point, the flow is turbulent only in the wake of the cylinder but laminar upstream and in the boundary layers.

At high Reynolds numbers, the flow separates from the surface of the cylinder and it is completely turbulent in the wake and in the boundary layer (see figure 2.1 (c)).

The critical value of Re for the flow to develop a fully turbulent wake is about 10^5.

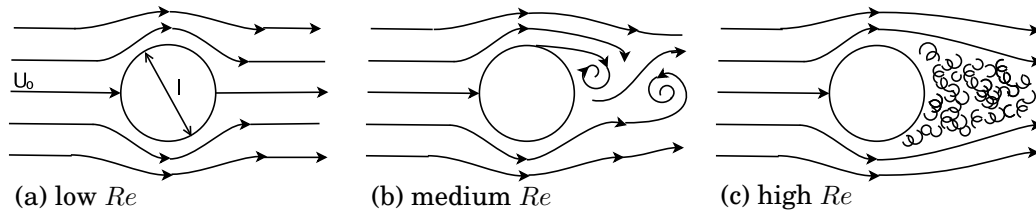(a) low Re (b) medium Re (c) high Re

Figure 2.1: Flow around a cylinder at different Reynolds numbers Re

The point where the flow separates from the surface is called the separation point. The position of this point on the surface of the cylinder depends mainly on the flow Reynolds number. Depending on the shape of the bluff body, the flow may form a separation bubble and reattach to the surface. The separation bubble is the region that enclosed the flow between the separation point and the reattachment point. The separation bubble is always associated with low pressure inside the bubble. Moreover the temperature of the flow in the separation bubble is higher than the surrounding flow temperature if the separation occurs next to a heated surface. This is because of some of the high temperature fluid might be trapped and circulating inside the separation bubble.

In case of high Reynolds number flow, there exists a broad spectrum of length scales. The largest vortices in the flow are characterized by the size of the body that created them. This is called the integral length scale l. The big scale eddies take their energy from the mean flow. They are unstable and they break up into smaller scale eddies, which themselves are unstable too, and they pass their energy to even smaller scale eddies. This is called the energy cascade and it is shown schematically in figure 2.2. The wide field of length scales η in the turbulent flow ranges from the integral length scale l to the smallest length scale of the flow.
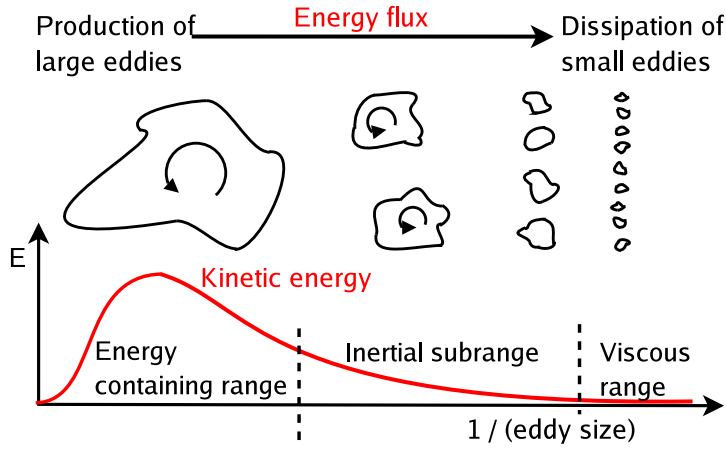
Figure 2.2: Energy cascade of a turbulent flow

Besides the length scale η there are two other scales of the motion, the time scale τ, the time which needs an eddy to turn over and the velocity scale v, which is $v = \eta/\tau$.

In the energy cascade, the viscosity plays no important part, as long as $Re = \frac{v\eta}{\nu} >> 1$. At those high Reynolds numbers the viscous forces can be neglected compared to the inertial forces, but when the vortex becomes small enough, the viscous forces are significant and the eddy disappears at the end. The energy of the vortex never disappears, but it is converted to internal energy of the flow by rising its temperature. The size of the smallest scales of the motion were described by Kolmogorov (1941). He premised, that they only depend upon the dissipation of kinetic energy ϵ and the kinematic viscosity ν. The Kolmogorov microscales are:

$$\eta_K \equiv (\nu^3/\epsilon)^{1/4}, \ \ \tau_K \equiv (\nu/\epsilon)^{1/2}, \ \ v_K \equiv (\nu\epsilon)^{1/4}. \tag{2.2}$$

Close to the solid boundaries, the scales of the flow are very small and they are of the same order of magnitude as the Kolmogorov microscales. The Reynolds number based on the turbulent scales in that region is very small and the dissipation of kinetic energy is very high.

2.1.1 Incompressible Flow

If the density ρ of all fluid particles is constant, then the flow is called incompressible flow. This does not imply that the density is the same

9

everywhere in the fluid. The density may be varying in space and time, but it must do so in precise way.

$$\frac{D\rho}{Dt} = \frac{\partial \rho}{\partial t} + u_j \frac{\partial \rho}{\partial x_j} = 0 \,, \qquad (2.3)$$

where t, u_j and x_j are the time, velocity of the flow and coordinates, respectively. No fluid is truly incompressible, but one may say a flow is almost incompressible, if the density variations of the fluid particles are negligibly small compared to the variation of flow velocity.

$$\frac{\partial \rho}{\partial x} << \frac{\partial u}{\partial x} \,. \qquad (2.4)$$

To decide whether to treat a flow as incompressible or not, the dimensionless Mach number M is useful. It compares the fluid velocity with the speed of sound,

$$M = \frac{\text{fluid velocity}}{\text{speed of sound}} = \frac{u}{a} \,. \qquad (2.5)$$

For ideal gas,

$$a = \kappa \frac{p}{\rho} = \sqrt{\kappa R T}$$

and equation 2.5 can be written as:

$$M = \frac{u}{\sqrt{\kappa R T}} \,, \qquad (2.6)$$

where κ is the ratio of specific heat, R is the gas constant and T is the temperature.
For $M < 0.2$, the flow is incompressible and subsonic. Thus one can say, the flow of liquids or gases is incompressible, if their velocity is small. The flow in ventilation ducts and the flow around automobiles can be considered to be incompressible and subsonic, for instance.

2.1.2   Governing Equations in Fluid Dynamics

The conservation laws can be applied to fluid dynamics to deduce equations governing the motion of the flow.
The continuity equation can be derived from the law of conservation

of mass, detailed explanations can be found in the book "Stroemungsmechanik" [14].

Using the Cartesian tensor notation, the resulting equation is:

$$\frac{\partial \rho}{\partial t} + \frac{\partial (\rho u_i)}{\partial x_i} = 0, \quad i = 1, 2, 3 \ . \tag{2.7}$$

For incompressible and Newtonian flow equation (2.7) can be written as:

$$\frac{\partial u_i}{\partial x_i} = 0 \ . \tag{2.8}$$

The principle of momentum conservation can be applied to the same fluid to deduce the momentum equations (Navier-Stokes equations). It can be written as a nonlinear partial differential equation:

$$\frac{\partial u_i}{\partial t} + u_j \frac{\partial u_i}{\partial x_j} = -\frac{1}{\rho} \frac{\partial p}{\partial x_i} + \nu \frac{\partial^2 u_i}{\partial x_j \partial x_j}, \tag{2.9}$$

where p is the instantaneous pressure. The kinematic viscosity ν and the dynamic viscosity μ are connected over ρ as follows:

$$\nu \equiv \mu/\rho \ . \tag{2.10}$$

The conservation of energy yields to the following equation for incompressible flow, neglecting heat transfer by radiation:

$$\frac{\partial T}{\partial t} + u_j \frac{\partial T}{\partial x_j} = \frac{\nu}{Pr} \frac{\partial T}{\partial x_j \partial x_j} + \frac{1}{c} \epsilon_{ij} \ , \tag{2.11}$$

where c is the specific heat capacity, which is a quantity of the fluid. The specific heat capacity c for air is about $1.005 \ \frac{J}{kg \ K}$. The variable ϵ represents the dissipation of energy. It is defined as:

$$\epsilon_{ij} = 2\nu \left(\frac{\partial u_i}{\partial x_k} \frac{\partial u_j}{\partial x_k} \right). \tag{2.12}$$

The properties of turbulent flow seem to fluctuate randomly. Statistical approach can be used after decomposing the flow into a mean part and a fluctuating part.

$$u = \overline{u} + u\prime \ ,$$
$$p = \overline{p} + p\prime \ ,$$
$$T = \overline{T} + T\prime \ .$$

In many cases, it is easier to analyse time averaged flow and to compare modified flow situations, while the instantaneous flow already differs

for the same flow problem over the time.

The time average of a flow variable as $f(\vec{x}, t)$ is defined by

$$\overline{f(\vec{x}, t)} = \lim_{\Delta t \to \infty} \frac{1}{\Delta t} \int_t^{t+\Delta t} f(\vec{x}, t)dt . \tag{2.13}$$

Using the decomposed variables of the flow, the continuity equations and the momentum equations can be written as the Reynolds averaged Navier Stokes equations:

$$\frac{\partial \overline{u_i}}{\partial x_i} = 0, \ \frac{\partial u_i'}{\partial x_i} = 0 \tag{2.14}$$

and

$$\rho \underbrace{\frac{\partial \overline{u_i}}{\partial t}}_{\text{time dependence}} + \underbrace{\rho \overline{u_j} \frac{\partial \overline{u_i}}{\partial x_j}}_{\text{convection}} = \underbrace{-\frac{\partial \overline{p}}{\partial x_i}}_{\text{pressure term}} + \frac{\partial}{\partial x_j} \big(\underbrace{\overset{=\mu}{\overbrace{\rho\nu}} \frac{\partial \overline{u_i}}{\partial x_j}}_{\text{viscous stress}} \underbrace{- \rho \overline{u_i' u_j'}}_{\text{Reynolds \"stresses\"}} \big). \tag{2.15}$$

The last term in equation (2.15) are the turbulent Reynolds stresses ($-\overline{u_i' u_j'}$). This term represents the influence of the turbulent motion on the averaged flow. There are no fluctuating scales in equation (2.15) since it is an equation for the averaged motion, however that makes it useful in studying turbulence. Due to the fact that the Reynolds stresses are unknowns, there are less available equations than demanded variables. Hence the big problem of equation (2.15) is a closure problem.

Neglecting the dissipation, the energy equation for time averaged flow can be written as:

$$\frac{\partial \overline{T}}{\partial t} + \frac{\partial \overline{T} \overline{u_j}}{\partial x_j} = \frac{\partial}{\partial x_j} \Big[\frac{\nu}{Pr} \frac{\partial \overline{T}}{\partial x_j} - (\overline{T} u_j' + T' \overline{u_j} + T' u_j') \Big]$$

$$= \frac{\partial}{\partial x_j} \Big[\frac{\nu}{Pr} \frac{\partial \overline{T}}{\partial x_j} - (\overline{T u_j} - \overline{T} \overline{u_j}) \Big]. \tag{2.16}$$

The letters Pr stand for the Prandtl number, which is a dimensionless quantity of the fluid. It describes the ratio between the kinetic viscosity to the conductibility of temperature.

2.2 Heat Transfer

There exists three different modes of heat transfer, conduction, radiation and convection.

- **Conduction**
  The conductive heat transfer is thermal diffusion due to the molecular motion inside solids, liquids and gases. The direction of the heat flux corresponds to the temperature gradient and is always from higher temperature to lower temperature on account of the second law of thermodynamics. The heat flow per unit time $\dot{Q}$ in x-direction through the x-normal Area A_x is:

$$\dot{Q} = -kA_x\frac{dT}{dx},\tag{2.17}$$

  where k is the conductivity constant that depends on the nature of the material and its temperature.

- **Radiation**
  A body with the temperature T emits over its faces of the area A to the environment with the temperature T_∞ the following heat per unit time:

$$\dot{Q} = \sigma\,\epsilon\,A\left(T^4 - T_\infty^4\right),\tag{2.18}$$

  with the Stefan-Boltzmann constant $\sigma = 5.67\cdot 10^{-8}\frac{W}{m^2K^4}$ and the specific emissivity $\epsilon \leq 1$.

- **Convection**
  The convective heat transfer happens due to the transport of particles in a flow, that are carrying their kinetic energy along. The convective heat transfer equation is:

$$\dot{Q} = hA(T - T_\infty),\tag{2.19}$$

  with the heat transfer coefficient h.
  A distinction is made between free or natural, and forced convection.
  Free convection explains motions of the fluid driven by buoyant forces that result from density differences. The density gradients are caused by temperature variations in the fluid.
  The term forced convection refers to heat transport that results from fluid motion caused by external means such as a pump, a fan, or atmospheric winds for instance.

Chapter 3

Numerical Methods of Flow Simulation

Direct Numerical Simulation (DNS), Reynolds-Averaged Navier Stokes Simulation (RANS) and Large Eddy Simulation (LES) are methods to numerically solve for the pressure p, the velocity u_i and the temperature T of the fluid in space and time.

3.1   Direct Numerical Simulation (DNS)

Doing Direct Numerical Simulations (DNS) means to numerically solve the governing equations of the flow to generate the exact instantaneous motions in a computer. These equations are the Navier Stokes equations (2.9), the continuity equation (2.8) and the energy equation. In case of incompressible flow is the energy equation not coupled with the continuity equation and the momentum equation. It is possible to first solve them and afterwards the energy equation using the results of the mean velocity field and the mean pressure to obtain the temperature field. In contrast, for compressible flow are these equations coupled and should be solved together.

We do not need any assumption or simplification for DNS, since we have as many equations as unknowns (u_i, p, and T). The problem of the DNS is, that the minimum vortex size that can be obtained from the numerical simulation is the size of the cell Δx. So to resolve all the scales of the flow, the cells should have the same size as the smallest scales in the flow, the Kolmogorov dissipation scales,

$$\eta_K \sim l \cdot Re^{-3/4} \, ,$$

where l is the integral length scale and Re is the Reynolds number based on the integral scales.

The number of cells needed for DNS increases with the Reynolds number. The time step Δt required for DNS should be very small to resolve the flow in time. There are two factors that control the choice of the time step. It should be smaller than the Kolmogorov time scale τ_K and in order to maintain numerical stability and accuracy, the time step should be small enough, that the fluid particles do not move more than one grid spacing in each time step. This yields:

$$\Delta t = \min(\tau_K, \tfrac{\Delta x}{u}).$$

Therefore DNS is restricted to low or moderate Reynolds numbers. For high Reynolds numbers, the flow is dominated with very fine structures associate with very small scales. The total number of cells needed to resolve all the scales is very high and hence the computational cost too. This makes DNS not feasible nowadays to solve high Reynold's number flow.

At low Reynolds numbers it is a useful tool in fundamental research of turbulence. Using DNS, one can perform "numerical experiments", and extract from them information difficult or impossible to get in the real laboratory, allowing a better understanding of the physics of turbulence.

However even if our computers were able to solve a more complicated flow in an adequate time, sometimes we would need to average the huge random data in order to understand turbulence.

It may sound easier to average the governing equations in the beginning and (2.9) and then to solve them afterwards. That could be done by simulating Reynolds-averaged Navier-Stokes equations (RANS).

3.2   Reynolds-Averaged Navier-Stokes (RANS)

In the Reynolds-Averaged Navier-Stokes equations (2.15), there are six extra terms, that take the fluctuating of the flow into account. These terms are called Reynolds-stresses. Hence there are more unknowns than equations. This is a manifestation of the *closure problem* and the reason why we need turbulence models.

There exists mainly two different kinds of turbulence models, the turbulent-

viscosity models and the Reynolds-stress models.

The turbulent-viscosity models act on the assumption that the Reynolds "stresses" could be acquired analogously to the viscous stress term, because it also resists the flow motion some how. This leads to:

$$-\overline{\rho u_i' u_j'} = \mu_t(\frac{\partial \overline{u}_i}{\partial x_j} + \frac{\partial \overline{u}_j}{\partial x_i}) - \frac{2}{3}\rho K \delta_{ij} . \qquad (3.1)$$

Here δ_{ij} is the Kronecker's delta, defined as:

$$\delta_{ij} = \begin{cases} 1 & \text{if } i = j \\ 0 & \text{otherwise} \end{cases} ,$$

and K, the kinetic energy is:

$$K = \frac{1}{2}\overline{u_i' u_i'}.$$

The second term on the right hand side of equation (3.1) is to balance the equation when $i = j$.

The turbulent dynamic eddy viscosity μ_t has to be modelled, it is not a property of the fluid, but a feature of the flow. It is not constant but it depends on position and time. Some models describe this with algebraic equations and some use partial differential equations.

The Reynolds-stress models characterise all the six terms separately by differential transport equations.

3.3 Large Eddy Simulation (LES)

Large eddy simulation (LES) decomposes the structures of the flow into large and small scales. The large motions of the flow are directly simulated but the influence of the small scale motions on the large scale motions are modelled. Hence LES is a kind of compromise between RANS and DNS.

The attributes of the coarse and the fine structures can be described as follows (quoting [15]):

coarse structured turbulence	fine structured turbulence
affected by the geometry of the flow	universal
inhomogeneous	homogeneous
anisotropic	isotropic
long-lasting	short-lasting
diffusive	dissipative
difficult to model	easier to model

The table above includes Kolmogorov's assumptions from 1941 about the energy cascade. These attributes are the reason, why it is useful to model only the small structures and simulate the big ones.

LES consists of four conceptual steps:

(i) Filtering
In this step, the actual velocity $u_i(\vec{x}, t)$ is decomposed into a filtered part and a subgrid component of velocity.

$$u_i(\vec{x}, t) = \underbrace{\overline{U}_i(\vec{x}, t)}_{\textbf{filtered component}} + \underbrace{U_i'(\vec{x}, t)}_{\textbf{subgrid-scale component}} , \qquad (3.2)$$

where $\overline{U}_i$ represents the motion of the large eddies and U_i' is the residual velocity field.
The temperature T is filtered as well:

$$T(\vec{x}, t) = \overline{T}(\vec{x}, t) + T'(\vec{x}, t).$$

(ii) Solving the filtered velocity field
The equations for the large scale eddies can be derived from the Navier-Stokes equations by inserting equation (3.2) and filtering that afterwards. It is analogously to the derivation of the Reynolds averaged Navier-Stokes equation, noticing that in general the filtered subgrid velocity does not equal zero and second filtering yields a different result from the first filtering:

$$\overline{U'}_i \neq 0 \text{ and } \overline{\overline{U}}_i \neq \overline{U}_i.$$

The filtered continuity and momentum equations for incompressible flow are:

$$\frac{\partial \overline{U}_i}{\partial x_i} = 0 , \qquad (3.3)$$

and

$$\rho\frac{\partial \overline{U_i}}{\partial t} + \rho\frac{\partial(\overline{\overline{U_j}\,\overline{U_i}} + \overline{U_i'U_j'} + \overline{U_i'\overline{U_j}} + \overline{\overline{U_i}U_j'})}{\partial x_j} = -\frac{\partial \overline{p}}{\partial x_i} + \mu\frac{\partial \overline{U_i}}{\partial x_j \partial x_j}. \quad (3.4)$$

The numerator of the second term in equation (3.4) can be reformulated as:

$$(\overline{\overline{U_j}\,\overline{U_i}} + \overline{U_i'U_j'} + \overline{U_i'\overline{U_j}} + \overline{\overline{U_i}U_j'}) =$$

$$\overline{U_i}\,\overline{U_j} + \overbrace{\overline{\overline{U_i}\,\overline{U_j}} - \overline{U_i}\,\overline{U_j}}^{\simeq 0} + \overbrace{\underbrace{\overline{U_i'U_j'}}_{\text{SGS Reynold stress}} + \underbrace{\overline{U_i'\overline{U_j}} + \overline{\overline{U_i}U_j'}}_{\text{cross term stress}}}^{=Q_{ij}} = \overline{u_i u_j}. \quad (3.5)$$

$$\underbrace{\phantom{\overline{\overline{U_i}\,\overline{U_j}} - \overline{U_i}\,\overline{U_j}}}_{\text{Leonard stress}}$$

If the Leonard stresses are neglected in equation (3.5), then equation (3.4) can be written as:

$$\rho\frac{\partial \overline{U_i}}{\partial t} + \rho\frac{\partial \overline{U_j}\,\overline{U_i}}{\partial x_j} = -\frac{\partial \overline{p}}{\partial x_i} + \frac{\partial}{\partial x_j}\left(\mu\frac{\partial \overline{U_i}}{\partial x_j} - Q_{ij}\right), \quad (3.6)$$

where Q_{ij} are the residual stresses defined as:

$$Q_{ij} = \overline{U_i'U_j'} + \overline{U_i'\overline{U_j}} + \overline{\overline{U_i}U_j'} = \overline{u_i u_j} - \overline{U_i}\,\overline{U_j}.$$

Similarly, the filtered energy equation arises as:

$$\frac{\partial \overline{T}}{\partial t} + \frac{\partial}{\partial x_j}(\overline{U_j}\overline{T}) = \frac{\nu}{Pr}\frac{\partial^2 \overline{T}}{\partial x_j \partial x_j} - \frac{\partial h_j}{\partial x_j}. \quad (3.7)$$

Here is h_j the unknown subgrid heat fluxes. They are defined as:

$$h_j = \overline{u_j T} - \overline{U_j}\overline{T}.$$

(iii) modelling the residual stress tensor and the subgrid heat fluxes

The turbulence models for the residual stresses are analog to the models used for the Reynolds stresses by RANS. The most simple one is proposed by Smagorinsky 1963, it neglects not only the Leonard-stress, but also the cross term stress. It models the SGS Reynold stress analogously to the eddy viscosity models.

$$Q_{ij} \simeq \overline{U_i'U_j'} = 2\nu_{SGS}\overline{S}_{ij}, \quad (3.8)$$

where S_{ij} is the resolved strain rate tensor, defined as:

$$\overline{S}_{ij} = \frac{1}{2}\left(\frac{\partial \overline{U}_i}{\partial x_j} + \frac{\partial \overline{U}_j}{\partial x_i}\right), \quad (3.9)$$

19

and ν_{SGS} is the subgrid scale viscosity that can be written as:

$$\nu_{SGS} = (C_S \Delta)^2 \sqrt{2\overline{S}_{ij}\overline{S}_{ij}}. \tag{3.10}$$

Here C_S is the model constant that is often called Smagorindky's
coefficient and ranges from 0.1 to 0.2. The subgrid scale Δ is the
cubic root of the volume of the cell, $\Delta = (\Delta_1\Delta_2\Delta_3)^{1/3}$. It should be
about the same magnitude as the filter width.
Using the Smagorinsky model, the subgrid heat fluxes can be
written as:

$$h_j = -\alpha_{SGS}\frac{\partial\overline{T}}{\partial x_j}. \tag{3.11}$$

Here, α_{SGS} is the subgrid scale eddy diffusivity and using Pr_{SGS}
for the subgrid Prandtl number, it is defined as:

$$\alpha_{SGS} = \frac{\nu_{SGS}}{Pr_{SGS}} = \frac{1}{Pr_{SGS}}(C_s\Delta)^2\sqrt{2\overline{S}_{ij}\overline{S}_{ij}}. \tag{3.12}$$

More information about subgrid-scale modelling can be found in
[16], [17] or [18].

(iv) numerically solve for the large eddy velocity
The last step is to solve the filtered equations (3.6) and (3.7 to get
the large eddy velocity field $\overline{U}_i$ and the Temperature $\overline{T}$.

The computing cost for LES is very low compared to that for DNS, since
one does not resolve all the turbulent scales in the flow. Contrary, in
DNS all the scales down to the Kolmogorov scales should be resolved.
In LES, the smallest scales are modelled and the grid spacing is ade-
quate being slightly smaller than the size of the smallest energy con-
taining motions.
Of course, the computational expense of LES is higher than for RANS,
but one can expect LES to be more accurate for flow in which large scale
unsteadiness is significant. The large scales dominate the transfer of
momentum, heat and chemical pollutants.

Chapter 4

Numerical Details

Large eddy simulations are made for the heat transfer and flow around a heated cube placed in the middle of a matrix of several cubes. Different simulations have been performed to investigate the influence of attaching vortex generators to the surface of the cube in the flow field and the heat transfer. This chapter describes the numerical details of the simulations. The size and design of the vortex generators and the computational meshes are explained.

4.1   Physical Model

The physical model is a heated cube placed in the middle of an equidistant matrix of surface-mounted cubes as shown in figure 4.1.
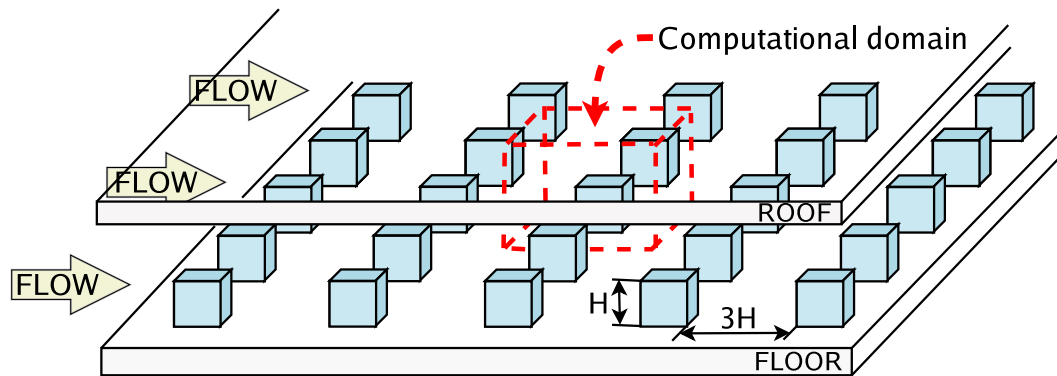
Figure 4.1: Central part of the Matrix of cubes mounted on a wall

The matrix of cubes is placed on one of the walls of a two-dimensional channel. It consists of a total of 25×10 cubes in the streamwise and spanwise directions, respectively. The side length of the cubes, H, is

15 mm. The height of the channel is 51 mm ($3.4H$). The distances between the centerlines of the cubes in the streamwise and the spanwise directions are 60 mm ($4H$).

4.2 Computational Domain and Boundary Conditions

The size of the computational domain is $4H \times 3.4H \times 4H$ as shown in figure 4.2. Similar to the experimental setup of Meinders and Hanjalić [2], the test cube is chosen to be in the middle of the matrix of cubes where the flow is fully developed in both the streamwise and the spanwise directions. Due to the periodicity of the flow around the cubes, periodic boundary conditions are applied in the streamwise and the spanwise directions for the velocity field. No-slip boundary conditions are employed at solid the walls.
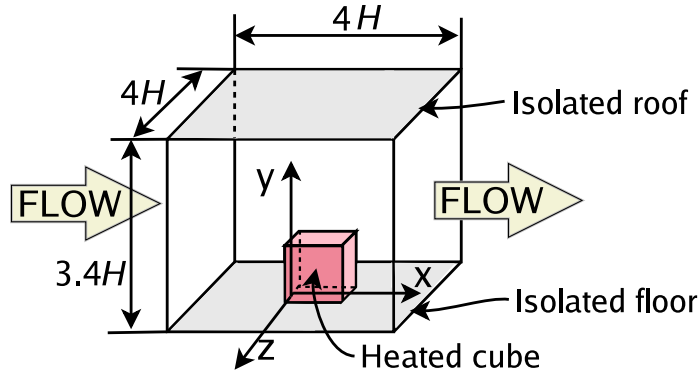

Figure 4.2: The computational domain

The x- and y-axis are taken in the streamwise and floor-normal directions, respectively while the z-axis denotes the spanwise direction. The coordinate system originates at the channel floor, where the center of the grounded edge of the cubes windward face is located, as shown in figure 4.2. The bulk velocity u_{bi} of the incoming flow is 3.86 m/s. It is the velocity of the mean flow, defined as:

$$u_{bi} = \frac{1}{A_i} \int\limits_{(A_i)} u(\vec{x})\, dA_i \,.$$ (4.1)

Here A_i is the area of the channel inlet, $3.4H \times 4H$, and $u(\vec{x})$ is the time-averaged velocity at the inlet of the cahnnel.

This yields to the value of the Reynolds number of 13100, based on the incoming bulk velocity and the height of the channel. If the Reynolds number is based on the size H of the cube, then its value is 3860. The density of the air is 1.16 kg/m^3 and its dynamic viscosity is $1.5 \times 10^{-5} \text{ m}^2/\text{s}$. A constant mass flow rate $\dot{m}$ of 0.0137 kg/s is passing the sub channel. The value of the Prandtl number of the air is 0.71.

4.3 Heat Transfer between the Cube and its Environment

The different modes of heat transfer, as conduction, radiation and convection, are described in chapter 2.2. This section here is about the specific details of the cooling cube and its heat transfer with the environment.

The rate of heat dissipated from an individual cube to the air, $\dot{Q}$, is constant and equal to 2 Watt. It implies a constant heat flux of 1777.8 W/m^2 through the cubes surfaces. This makes the temperature rise between any two successive cubes to be constant. Periodic boundary conditions for the temperature and temperature rise are applied in the spanwise and streamwise directions, respectively. The investigated model includes heat transfer in a periodically repeating geometry and since the thermal boundary conditions are of the constant wall heat flux type, periodic thermal conditions may be established, referring to the fluent6.2 documentation [19].

The bulk temperature T_{bi} for the incoming flow is 294 K. It is defined as a temperature average, that takes the different mass flow $\dot{m}$ over the inlet area A_i in account,

$$T_{bi} = \frac{1}{\dot{m}} \int \dot{T} \, d\dot{m} = \frac{\int\limits_{(A_i)} \rho u T \, dA_i}{\int\limits_{(A_i)} \rho u \, dA_i}. \tag{4.2}$$

Conservation of energy between inlet and outlet leads to the bulk temperature at the outlet T_{bo} with the following equation:

$$\dot{Q} = (T_{bo} - T_{bi})\dot{m}c_p, \tag{4.3}$$

where c_p is the specific heat of the fluid. In case of air, it is approximately 1000 $\frac{J}{kg\,K}$. It yields to the outlet bulk temperature of 294.146 K and a bulk temperate difference between in- and outlet less than 0.146 K. The channel walls are insulated and there is no heat flux through the

small faces of the vortex generators, which are explained below in section 4.5.

The effects of heat transfer by radiation from the different cubes are assumed to be negligible small. To ensure that this is an acceptable simplification, the heat that could be emitted from the varied cubes per unit time is calculated below.

$$\dot{Q} \; = \sigma \, \epsilon \, A \left(T^4 - T_\infty^4 \right), \qquad \text{with} \, (\epsilon \leq 1),$$

$$\Rightarrow \; \dot{Q} \; \leq \sigma \, A \left(T^4 - T_\infty^4 \right), \qquad \text{where } T = T(\vec{x}, t).$$

For the time-averaged heat flux follows:

$$\Rightarrow \; \overline{\dot{Q}} \simeq \sigma \left(\int_A \overline{T^4} \, dA - A \, T_\infty^4 \right), \tag{4.4}$$

$$\overline{T^4} = \overline{(\overline{T} + T')^4} = \overline{T}^4 + 4\overline{T}^3 \cdot \underbrace{\overline{T'}}_{=0} + 6\overline{T}^2 \cdot \overline{T'^2} + 4\overline{T} \cdot \underbrace{\overline{T'^3}}_{\simeq 0} + \overline{T'^4}.$$

The fluctuating temperature T' is much smaller than the mean vallue of the temperature $\overline{T}$, hence to simplify and to get an approximation for the vallue of the time-averaged heat flux $\dot{Q}$, the terms including T' are less important. It follows:

$$\overline{T^4} \approx \overline{T}^4. \tag{4.5}$$

Table 4.1 lists the computed values for the time-averaged heat that could be emitted by the cubes approximative. It shows that radiation is not very important and to simplify the investigated heat-transfer problem, it can be neglected.

	Cube without VG	Cube with VG1	Cube with VG2
$\int_A \overline{T}^4 \, dA \quad [K^4 m^2]$	$1.378 \cdot 10^7$	$1.324 \cdot 10^7$	$1.234 \cdot 10^7$
$\overline{\dot{Q}} \qquad [W]$	0.305	0.274	0.223

Table 4.1: Table of the approximated time-averaged heat emitted by the cubes

The following discusses, if the effects of free convection are also negligible or if combined effects of free and forced convection must be considered.

The Grashof number Gr is a ratio of the buoyancy forces to the viscous forces acting on the fluid. The root of the Grashof number $Gr^{1/2}$ plays the same role in free convection as the Reynolds number Re in forced convection, since the Reynolds number is the ratio of the inertial to viscous forces acting on the fluid. Hence, if $Gr/Re^2 \approx 1$, free and forced convection are influencing the heat transfer in similar intensity. One may neglect the free convection, if $Gr/Re^2 \ll 1$. Conversely, forced convection effects are negligible, if $Gr/Re^2 \gg 1$.

Based on the size of the cube, the Grashof number Gr_H can be written as [20]:

$$Gr_H = \frac{g\beta(T - T_\infty)H^3}{\nu^2}. \tag{4.6}$$

Here, g is the acceleration due to gravity. On earth its value is about $9.81 \, \text{m/s}^2$. The coefficient β is known as the volumetric thermal expansion coefficient and is defined as:

$$\beta = -\frac{1}{\rho}\left(\frac{\partial \rho}{\partial T}\right)_{p=\text{const}}. \tag{4.7}$$

If the fluid is an ideal gas, $\rho = p/RT$, then it follows:

$$\beta = -\frac{1}{\rho}\left(\frac{\partial \rho}{\partial T}\right)_{p=\text{const}} = \frac{1}{\rho}\frac{p}{RT_\infty^2} = \frac{1}{T_\infty}. \tag{4.8}$$

The temperature T at the surface of the cube is always lower than $370K$. Now, the equation (4.6) can be rearranged and the Grashof number can be estimated:

$$Gr_H \approx \frac{g(T - T_\infty)H^3}{T_\infty\nu^2} \leq \frac{9.81m/s^2 \cdot (370K - 294K) \cdot (15mm)^3}{(1.5 \cdot 10^{-5}m^2/s)^2 \cdot 294K} = 3.804 \cdot 10^4. \tag{4.9}$$

The Reynolds number Re_H based on the height of the cube H and the bulk velocity of the incoming flow u_{bi} is:

$$Re_H = \frac{u_{bi}H}{\nu} \approx 3860. \tag{4.10}$$

Hence, the ratio of the buoyancy forces to the inertial forces is:

$$Gr_H/Re_H^2 \approx 2.55 \cdot 10^{-3} \ll 1, \tag{4.11}$$

and the effects of the free convection may be neglected.

The remaining modes of heat transfer for the investigated problem of cooling down surface mounted cubes are forced convection and conduction.

4.4   Equations for LES

For the investigated case of flow simulation, it is assumed to have incompressible conditions. Hence the Mach number should be smaller than 0.2, as explained in chapter 2.1.1. For air the value of κ is 1.4 and R is $287\frac{J}{kg\ K}$. The temperature is at least $294K$ and the incoming fluid velocity u_b is 3.86 m/s. The expected maximum of the velocity is four times the bulk velocity. Therefore the Mach number M, based on the maximum velocity, can be estimated as follows:

$$M \leq \frac{u_b \cdot 4}{\sqrt{\kappa R T}} = \frac{3.86 m/s \cdot 4}{\sqrt{1.4 \cdot 287\frac{J}{kg\ K} \cdot 294K}} = 0.04. \tag{4.12}$$

It is distinguishable that incompressible flow can be assumed (see section 2.1.1).

4.4.1   The Filtered Continuity, Momentum and Energy Equations

The filtered equations that are used in LES to derive the velocity and temperate fields are explained in section 3.3, "Large Eddy Simulation (LES)".
The filtered continuity equation for incompressible flow is:

$$\frac{\partial \overline{U}_i}{\partial x_i} = 0\,. \tag{4.13}$$

Choosing the model constant C_s to be 0.1, the following filtered momentum equation is used:

$$\rho\frac{\partial \overline{U}_i}{\partial t} + \rho\frac{\partial \overline{U}_j \overline{U}_i}{\partial x_j} = -\frac{\partial \overline{p}}{\partial x_i} + \frac{\partial}{\partial x_j}\Big[\mu\frac{\partial \overline{U}_i}{\partial x_j} - (C_S\Delta)^2\sqrt{2\overline{S}_{ij}\overline{S}_{ij}}\Big(\frac{\partial \overline{U}_i}{\partial x_j} + \frac{\partial \overline{U}_j}{\partial x_i}\Big)\Big] \tag{4.14}$$

LES is done to solve for the temperature field after solving for the velocity field, since these equations are not coupled for incompressible flow. The filtered equation for the heat transfer is:

$$\frac{\partial \overline{T}}{\partial t} + \frac{\partial}{\partial x_j}(\overline{U}_j \overline{T}) = \frac{\nu}{Pr}\frac{\partial^2 \overline{T}}{\partial x_j \partial x_j} + \frac{1}{\partial x_j}\Big(\frac{1}{Pr_{SGS}}(C_S\Delta)^2\sqrt{2\overline{S}_{ij}\overline{S}_{ij}}\Big). \tag{4.15}$$

Here, Pr is the Prandtl number of the air, 0.71, and Pr_{SGS} is the subgid scale Prandtl number. The value of Pr_{SGS} is set to be 0.6 in all the simulations.

4.5 Vortex Generators

There are three different cubes included in this work. One is just a simple smooth cube, but the two other cubes are varied to have vortex generators, little bodies mounted on their surfaces. The first is called vortex generator 1 (VG1) and the second is vortex generator 2 (VG2).
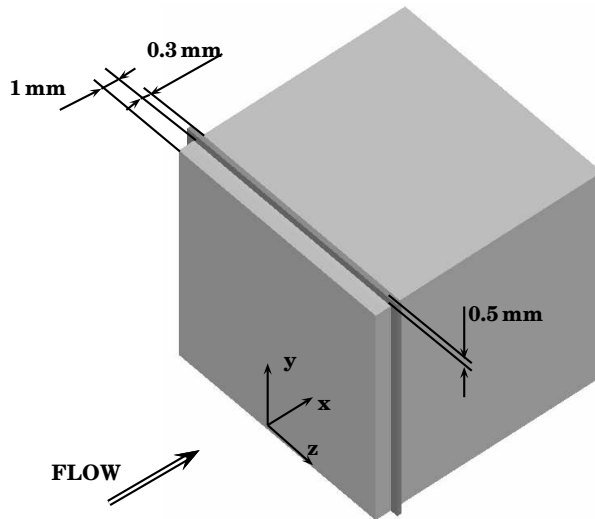

Figure 4.3: The shape of the vortex generator 1

VG1 is a simple rib attached to the side and top faces of the cube at a distance 1 mm from the windward edge of the cube. This position corresponds to the start of flow separation at the side and top faces of the cube without any vortex generator. The thickness of the VG is 0.3 mm and its height is 0.5 mm. Figure 4.3 shows the details of the shape of VG1.

The VG2 consists of five small cubes at the top side and at each of the lateral sides. This leads to a total number of 15 small cubes attached to the surface of the big cubes. The small cubes are placed 1 mm apart from the front edge of the big cube like the VG1. They have the same thickness and height as the VG1 of 0.3 mm and 0.5 mm, respectively. The width of these small cubes is 0.5 mm and the gap between is 2 mm. Without the gaps between the small cubes, VG2 would be the same as VG1. The geometric design of VG2 can be seen in figure 4.4.
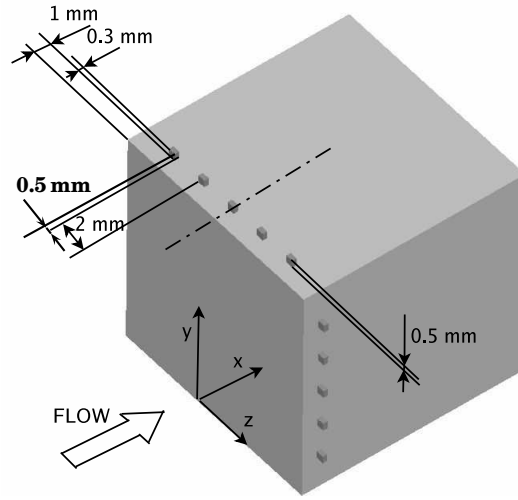
Figure 4.4: The shape of the vortex generator 2

4.6   Mesh

Three structured meshes are used for the simulations of the flow around the cube without a vortex generator, around the cube with VG1 and around the cube with VG2. The comercial software ICEM-CFD is used to generate the geometries and meshes. The meshes consist of $O-$ and $C-$grid topologies as shown in the figures (4.5) till (4.7). This makes it possible to have very fine mesh near the solid surfaces but coarse mesh in other parts. Hence it helps to have an adequate number of cells and to save computational time.

The meshed domain consists of different blocks to enable the creation of the desired whole grid with its different scales of cells.

There are 408,016 hexahedral cells forming the mesh for the cube without a VG. It is the mesh one can see in figure 4.5.

The grid around the cube with VG1 has 928,298 hexahedral cells. It is shown in figure 4.6.

The mesh used for the domain of the cube with VG2 has 431,064 hexahedral cells (see figure 4.7). Using $C-$ and $O-$grid topologynot only around the big cube but also around the small cubes, makes it possible to decrease the number of needed cells around the cube with VG2 compared with the mesh around the cube with VG1.

Since resolving the boundary layers is important in these simulations, the meshes are made very fine next to the solid walls.
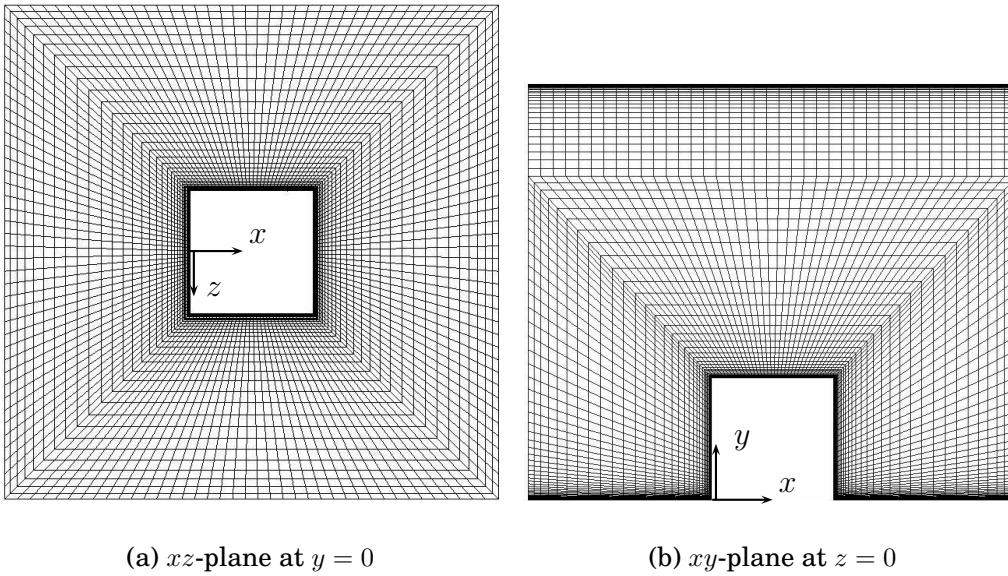
(a) xz-plane at $y = 0$ (b) xy-plane at $z = 0$

Figure 4.5: The grid around the cube with no VG

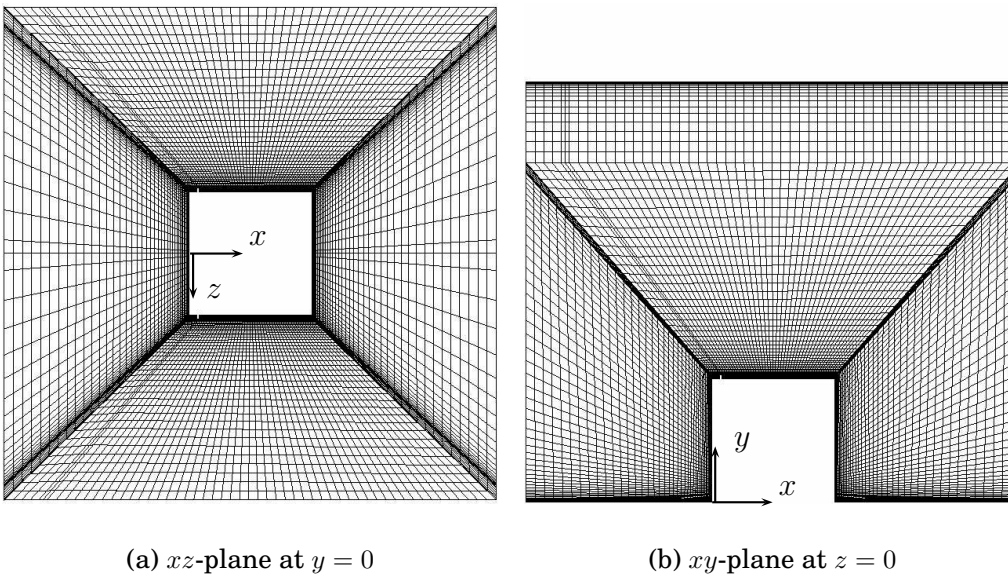(a) xz-plane at $y = 0$ (b) xy-plane at $z = 0$

Figure 4.6: The grid around the cube with VG1

The turbulent boundary layer can be divided into different regions. Experimental data of Laufer [21] shows that close to the wall there is a region, where the Reynolds-averaged momentum equations (2.15) can

be reduced to:

$$u_*^2 \approx \nu \frac{\partial \overline{u}}{\partial y}. \tag{4.16}$$

u_* is the friction velocity, defined as:

$$Here, u_*^2 \equiv \frac{\tau_W}{\rho}, \tag{4.17}$$

with the wall-shear stress

$$\tau_W \equiv \mu \frac{\partial \overline{u}}{\partial y}\bigg|_{y=0}. \tag{4.18}$$

It is called the linear sublayer because of the linear mean-velocity profile. If the centers of the first layer of cells are in that region, then the mesh is not too course and the flow can be resolved in this part. The thickness of the linear sublayer is usually expressed with the non-dimensional coordinate y^+:

$$y^+ \equiv \frac{yu_*}{\nu},$$

where y is the physical wall-normal distance between the center of the boundary cell and the wall. Experimental data shows, that the extent of the linear sublayer is $y^+ = 3$ (see [22]).

The centers of the boundary cells of the cube with vortex generator 1 have at most the displacement y of $3.5 \cdot 10^{-5}$ m and the wall-shear stress τ_W is everywhere at the walls less than $1.62 \ N/m^2$. As a consequence, $y^+ < 2.7$.

For VG2 the normal distance y between the wall and the center of the first cell is always smaller than $6.5 \cdot 10^{-6}$ m and the wall-shear stress τ_W at the cube and the roof and floor is smaller than $3.06 \ N/m^2$. These values leads to a maximal y^+ of 0.71. Hence the resolution of the meshes for the cube with VG1 and the cube with VG2 should be very good.

It is desired not to have influence of the mesh in the results of neither the flow nor the heat transfer.

To assure that these results are independent of the mesh, a second mesh is generated around the cube with vortex generator 2. That new mesh, shown in figure 4.8, is finer than the first one and hence it has more cells. The fine mesh has 761,277 nodes and 737,664 hexahedral cells. The number of cells of the fine mesh is almost twice times bigger than the number of the cells of the first coarser mesh. The results of the simulations with to different meshes have to be compared with each other.
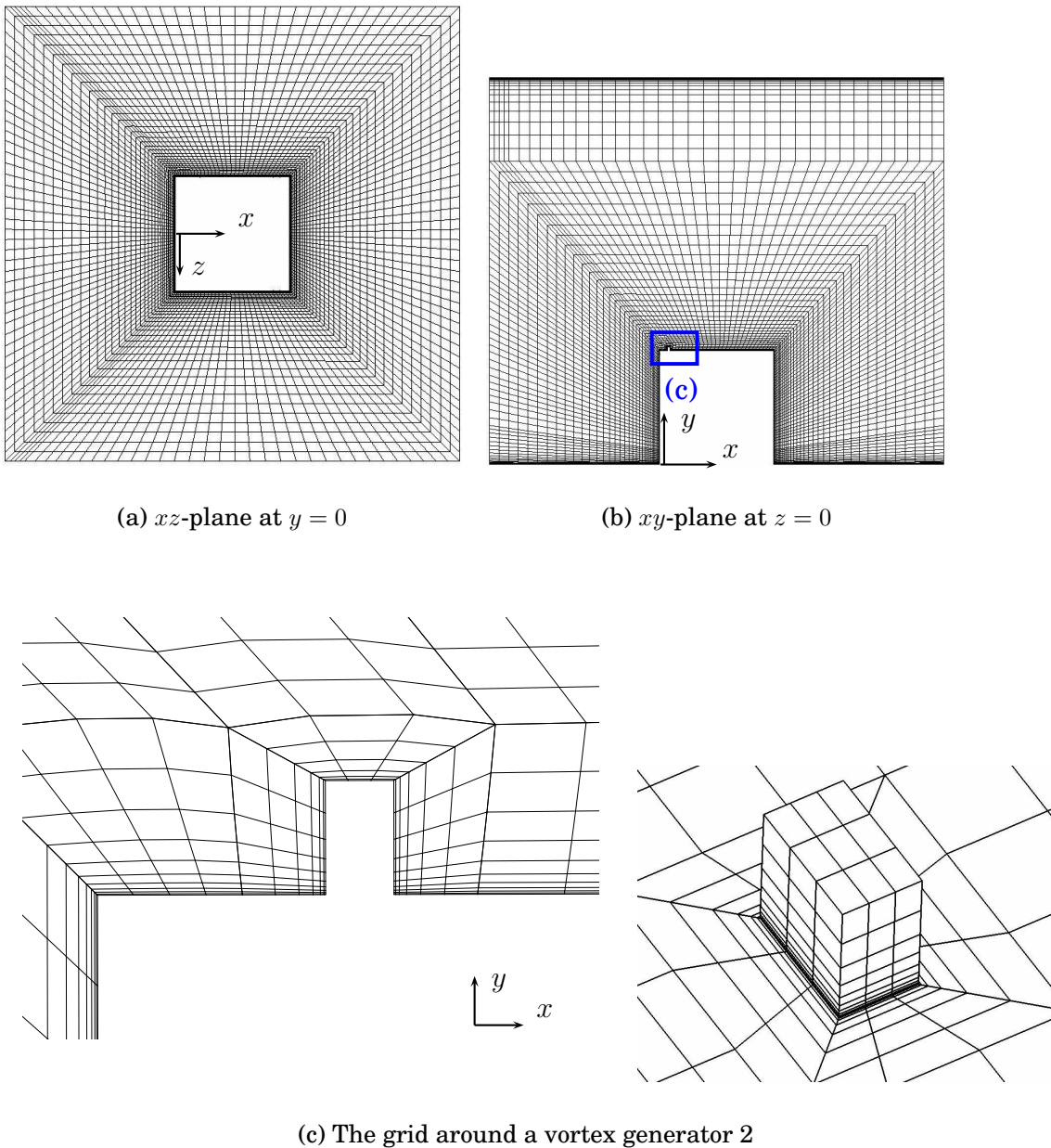
(a) xz-plane at $y = 0$

(b) xy-plane at $z = 0$

(c) The grid around a vortex generator 2

Figure 4.7: The grid around the cube with VG2

4.7 Computational Fluid Dynamics (CFD)

The derived filtered equations (4.13), (4.14) and (4.15) are solved numerically for the discrete domain of finite parts. The method of finite
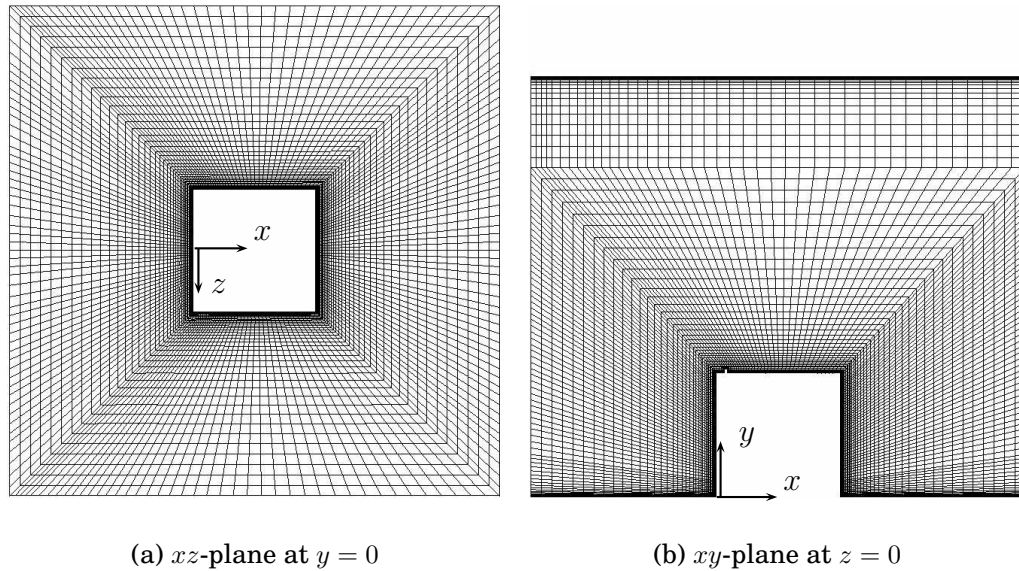
(a) xz-plane at $y = 0$ (b) xy-plane at $z = 0$

Figure 4.8: The finer second mesh around the cube with VG2

volumes (FVM) concentrates all the properties of the cell at the center of it. Hence there emerges one linear equation for each cell and a resulting system of equations has to be solved. Fluent does this in an iterative way. It uses the tridiagonal matrix algorithm (TDMA), also known as the Thomas algorithm, which is a simplified form of the Gaussian elimination method. Only for the discretisation of 1D problems arises really a matrix with three diagonals, but for 2D there are five diagonals and for 3D there are seven diagonals. This means, that there are more steps needed to solve the equations of a 3D than of a 1D problem, even though the number of cells would be the same.
The number of time steps is at least 20,000 for each of the simulations.

Chapter 5

Results

This chapter addresses the results of the different simulations. Mesh-independency is shown in the first section. The validation of the numerical simulations is done by comparison with the available experimental data. The rest of the chapter shows the contrast between the results that obtained from the different simulations. The comparisons investigate the influence of vortex generators on the flow field and the heat transfer.

5.1 Validation of the Results

5.1.1 Comparison between Results of the Fine and the Coarse Meshes

Two large eddy simulations with a fine mesh and a coarser mesh around the cube with vortex generator 2 were made to show the results' independence of the grid. A constant mass flow rate of 0.0174 kg/s was used in these computations.

Figure 5.1 shows nine profiles of the mean streamwise velocity and the mean temperature of the air for each of the two meshes beginning at $z = 0$ and ending at $z/H = 2$. The first two figures 5.1 (a) and (b) include the results in front of the cube at the height of $y/H = 1/2$ and the streamwise position of $x/H = -1/2$ and $x/H = -1/4$, respectively. Then there are five profiles from above of the cube at the height of $y/H = 1.01$ and two profiles behind the cube at the height of $y/H = 1/2$ again. The mean temperature profiles (black) are very similar for the fine (dashed line) and the coarse (solid line) mesh, the difference is mostly less than $1K$. The agreement of the data of the mean x-velocity (grey) is even better as one can see in that figure 5.1.

(a) $x/H=-\frac{1}{2}$, $y/H=\frac{1}{2}$

(b) $x/H=-\frac{1}{4}$, $y/H=\frac{1}{2}$

(c) $x/H=\frac{1}{10}$, $y/H=1.01$

(d) $x/H=\frac{1}{4}$, $y/H=1.01$

(e) $x/H=\frac{1}{2}$, $y/H=1.01$

(f) $x/H=\frac{3}{4}$, $y/H=1.01$

(g) $x/H=1$, $y/H=1.01$

(h) $x/H=\frac{5}{4}$, $y/H=\frac{1}{2}$
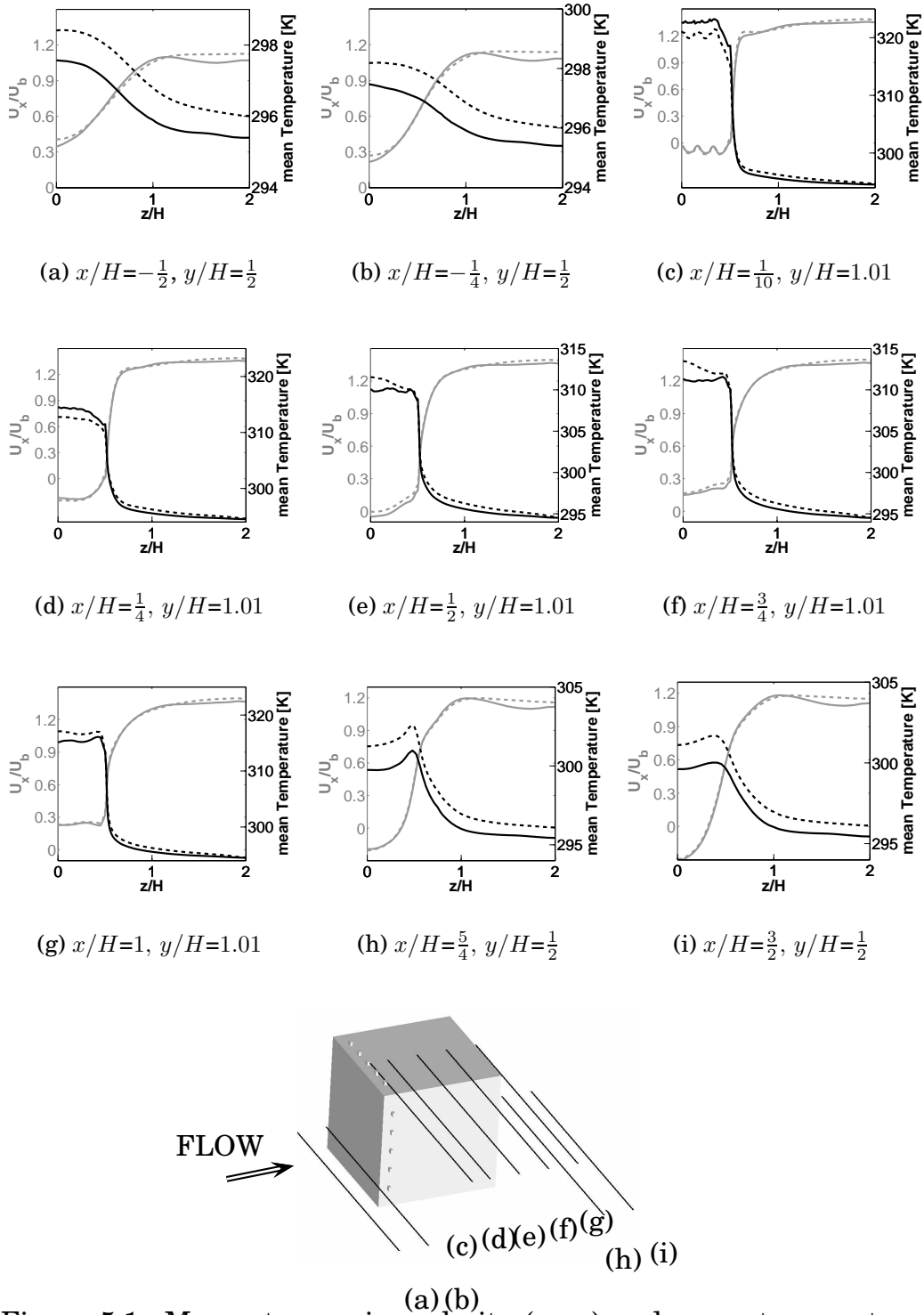
(i) $x/H=\frac{3}{2}$, $y/H=\frac{1}{2}$

Figure 5.1: Mean streamwise velocity (grey) and mean temperature (black) profiles for the cube with VG2. Solid line: coarse mesh; dashed line: fine mesh.
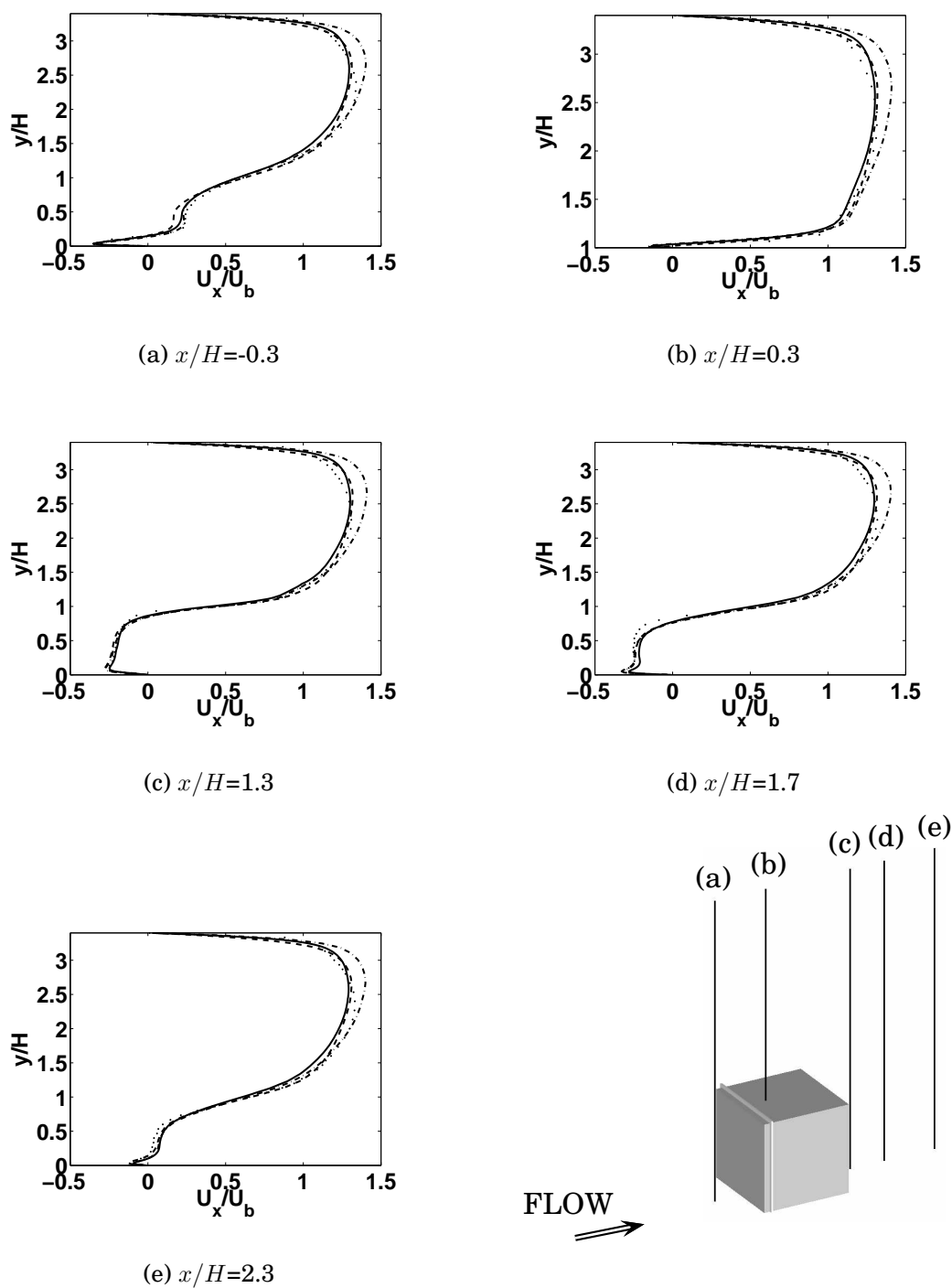
(a) x/H=-0.3

(b) x/H=0.3

(c) x/H=1.3

(d) x/H=1.7

(e) x/H=2.3

Figure 5.2: Streamwise velocity profiles in the vertical xy-plane at z/H=0. Dots: experimental results for a smooth cube (Meinders [2]); LES: solid line: smooth cube; dashed line: cube with VG1; dash-dot line: cube with VG2.

The differences of the two results from the varied meshes are small enough to be neglected and hence, the resolution of the coarse mesh is fine enough to use it for the comparison between the cubes with and without vortex generator.

5.1.2   Comparison with Experimental Results

The results of the experiments of Meinders [2] for a smooth cube are used to validate the LES data. But there are no experiments found about cooling cubes having vortex generators attached to their surfaces.

Figure 5.2 shows the streamwise velocity distribution on the vertical $xy-$plane at z/H=0 at five different locations in the streamwise direction. The profiles of the cube without vortex generator of the experimental data and the LES data show good agreement, verifying that the mesh resolution is fine enough to resolve the flow and hence the heat transfer.

5.2   Time-Averaged Flow

The streamlines of the time-averaged flow might show a difference for the three varied cubes.

(a) Cube without vortex generator

(b) Cube with vortex generator 1

(c) Cube with vortex generator 2
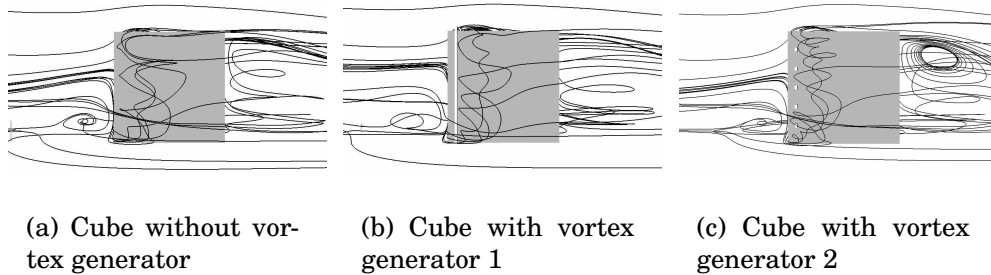
Figure 5.3: time-averaged streamlines around the different cubes

One can see the three dimensional time-averaged streamlines in figure 5.3. It is very complex and difficult to compare these lines for the cube without a VG, figure 5.3 (a), with the lines for the cubes with VG1 and VG2, figure 5.3 (b) and figure (c), in 3D. Thus, the following

(a) Cube without vortex generator

(b) Cube with vortex generator 1
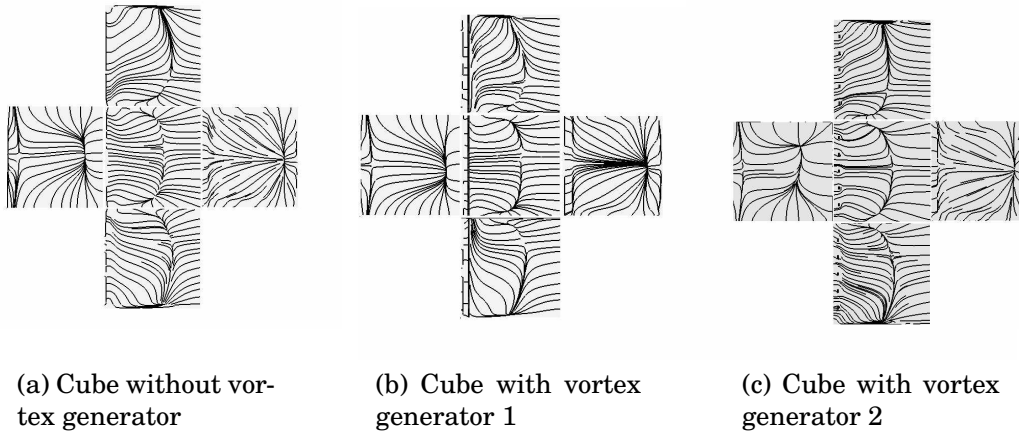
(c) Cube with vortex generator 2

Figure 5.4: time-averaged streamlines projected on planes parallel to the faces of the cube with a normal distance of $0.0001H$.

describes the time-averaged streamlines in some planes instead of 3D.

The time-averaged streamlines are projected on planes parallel to the faces of the cubes with a very small distance of $0.0001H$ as shown in figure 5.4.
The streamlines projected at the cube without vortex generator (figure 5.4 (a)) and those which are projected at the cubes with VG1 and VG2 (figure 5.4 (b) and (c)) still look very similar.

Figure 5.5 shows the time-averaged streamlines around the cube without a vortex generator, the cube with vortex generator 1 and the cube with vortex generator 2 in the plane $y/H = 0.5$.
The whole pictures seem to be very similar. There is always a separation region at the lateral sides of the cube that begins at the front edges. Later on the flow reattaches to the surfaces and then separates again at the back edge. It forms a big bubble in the wake and generates a saddle point in the end, marked with a red cross in figure 5.5. The distance from the lee side to this point varies only slightly. For the cube without a VG it is $1.087H$, for the cube with VG1 it is $1.095H$ and for the cube with VG2 it is $1.143H$. That small difference in one plane could still represent an important change for the 3D case.

Another difference between these three figures of the time-averaged streamlines can be seen, if one looks more precisely at the lateral separation bubble. figure 5.6 zooms in these bubbles.

37

(a) Cube without vortex generator

(b) Cube with vortex generator 1

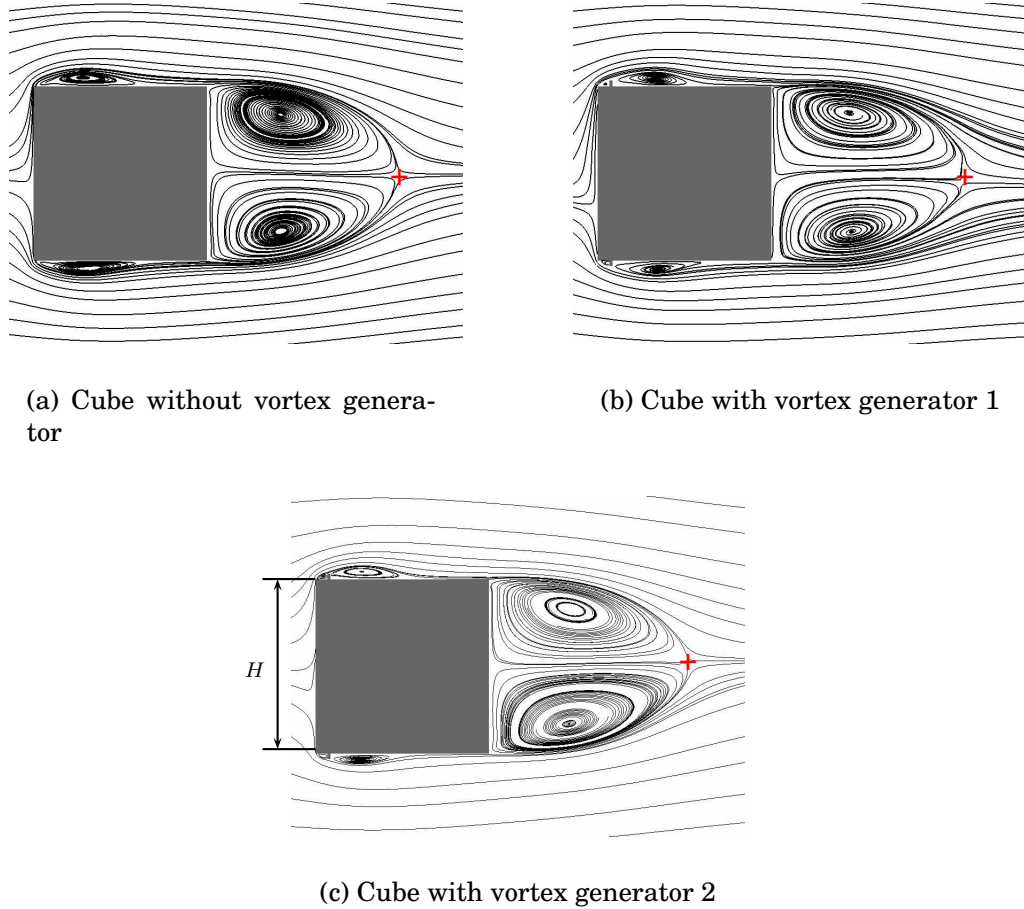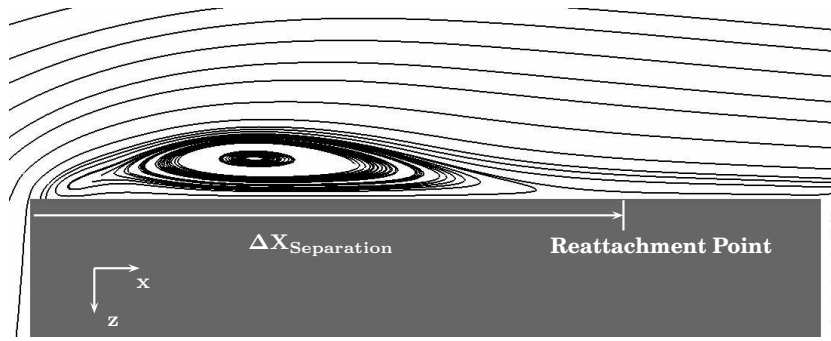

(c) Cube with vortex generator 2

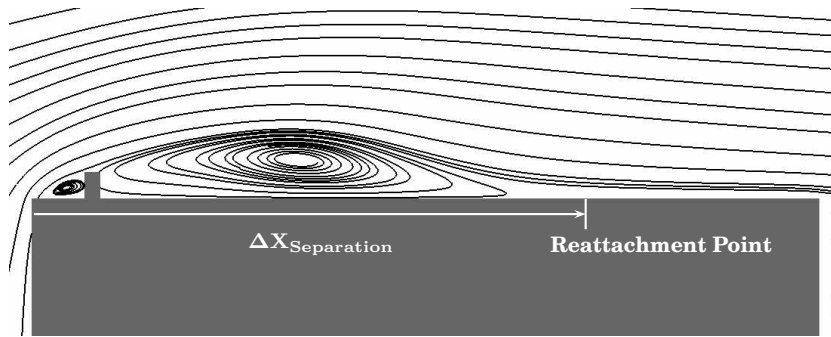Figure 5.5: Time-averaged streamlines at the plane $y/H = 0.5$.

The reattachment of the flow at the lateral sides of the cubes at $y/H = 0.5$ is not the same for the different cases. Figure 5.6 shows that the distance from the front edge until the end of separation $\Delta X_{Separation}$ is largest for the cube without a vortex generator (figure 5.6 (a)) and smallest for the cube with VG2 (figure 5.6 (c)). The value of $\Delta X_{Separation}$ for each cube is listed in table 5.1.

	Cube without VG	Cube with VG1	Cube with VG2
$\Delta X_{Separation}/H$	0.75	0.70	0.65

Table 5.1: Length of the separation at the lateral side of the cube at the plane $y/H = 0.5$, corresponding to figure 5.6

(a) Cube without vortex generator

(b) Cube with vortex generator 1
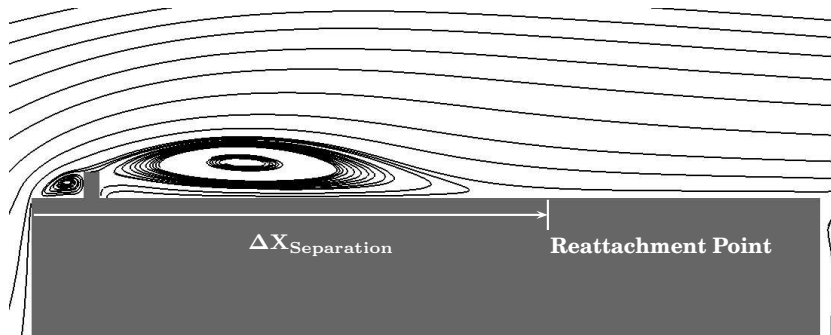
(c) Cube with vortex generator 2

Figure 5.6: Time-averaged streamlines of the flow at the lateral sides of the cubes at the plane $y/H = 0.5$

Figure 5.6 and table 5.1 demonstrate, that the vortex generators shortens the distance of flow separation.

The three dimensional streamlines, displayed in figure 5.3 show that there is a difference in the incoming flow, which is caused by the changes of the wake of another cube. In front of the cube, one part of the flow moves upwards, another part goes to the left and right of the cube and the remaining flow that is confronted with the cube surface turns its direction down. When this part reaches the ground, it has to change its route again. Doing so, it is forming a bubble.

It might be interesting to compare those flow structures in front of the cubes for the variable cases. Streamlines in the plane z=0, that cuts the cube vertically in its center, are chosen in figure 5.7.

The time-averaged flow splits at the front sides of the cubes upwards and downwards. The height of that stagnation line differs. It is largest for the cube with VG1 (figure 5.7 (b)) and smallest for the cube with VG2 (figure 5.7 (c)). Table 5.2 lists the exact values.

	Cube without VG	Cube with VG1	Cube with VG2
$\Delta y_{down}/H$	0.8	0.86	0.65

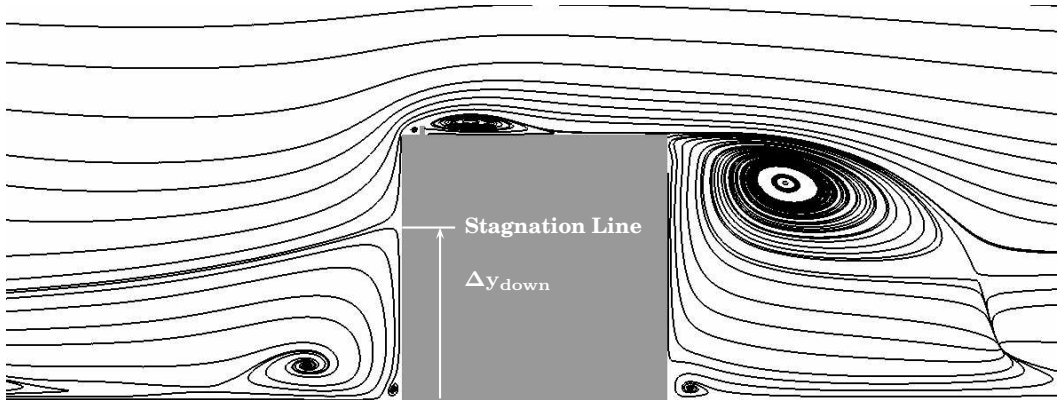Table 5.2: Height of the stagnation line at the front side of the cube in the plane z=0

The analysis of the time-averaged streamlines shows a difference in the flow around the smooth cube and the cubes with vortex generators. These differences certainly influence the convective heat transfer process.
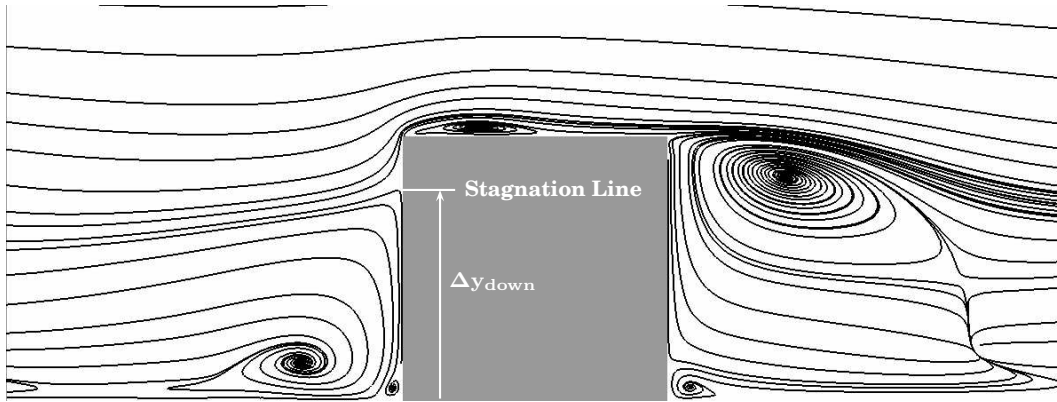
(a) Cube without vortex generator
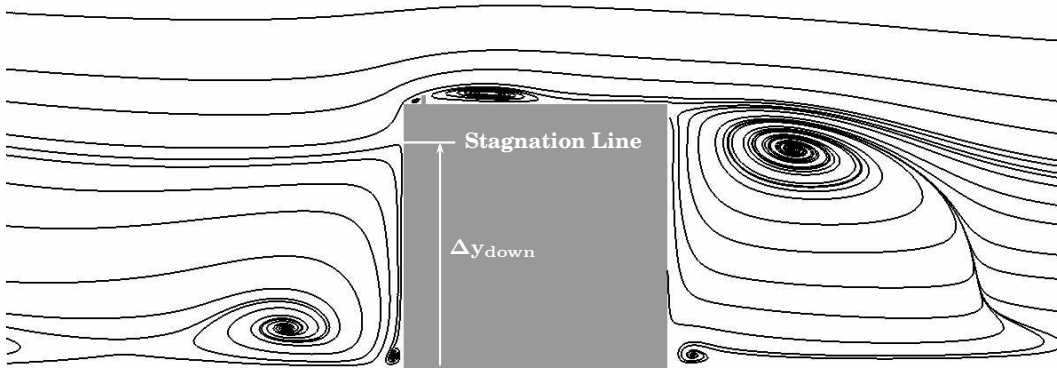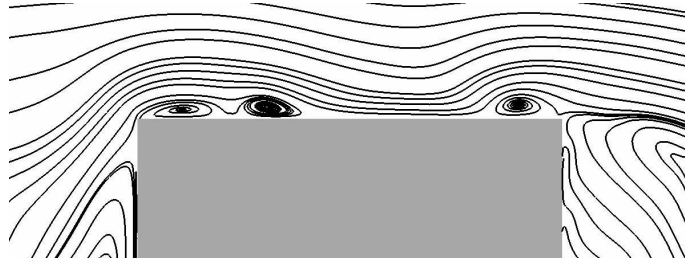

(b) Cube with vortex generator 1

(c) Cube with vortex generator 2

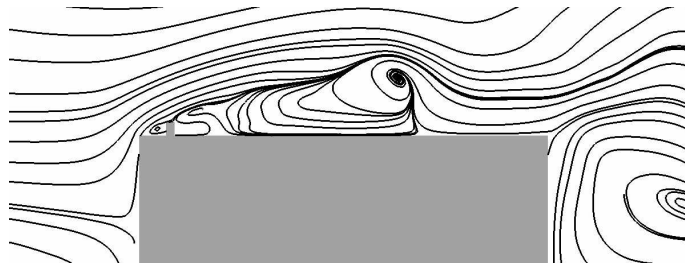Figure 5.7: Time-averaged streamlines in the plane z=0

5.3   Instantaneous Flow

In this section, the instantaneous flow around the varied cubes is investigated to show the differences that appear due to the existence of vortex generators.
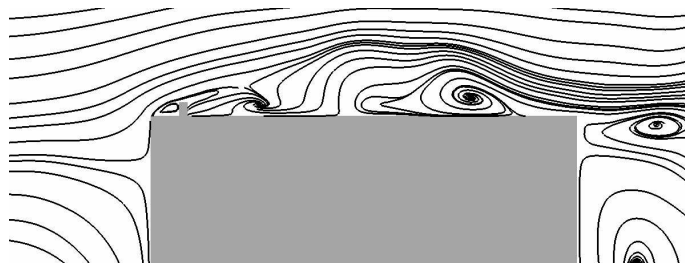
Figure 5.8 shows instantaneous streamlines close to the lateral face of the cube.

(a) Cube without vortex generator
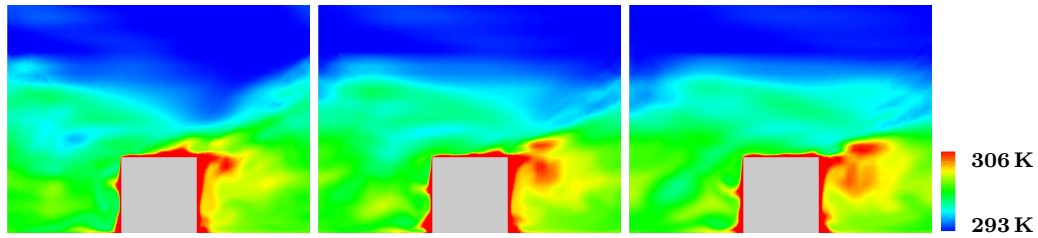

(b) Cube with vortex generator 1

(c) Cube with vortex generator 2

Figure 5.8: Instantaneous streamlines in the plane y/H=0.5

Because of the vortex generators, there is a different boundary layer on the surface of the cubes than on the cube without any VG. The new

boundary layer is dominated with vortices that are more turbulent and more unsteady. This leads to an increasing heat transfer while these structures help to carry the heat from the surface and the viscous sub-layer to the bulk flow.
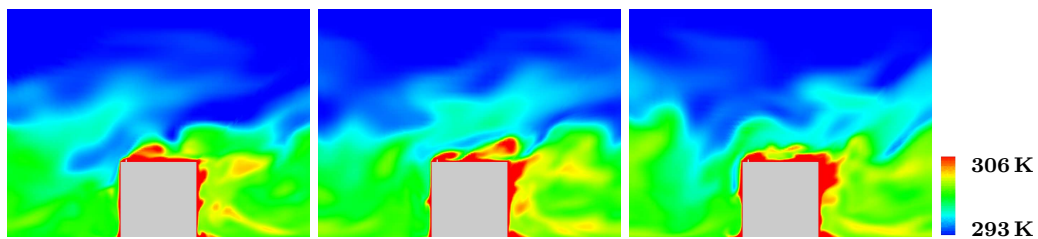
The temperature distributions around the cubes are shown in fig-

(a) Cube without vortex generator
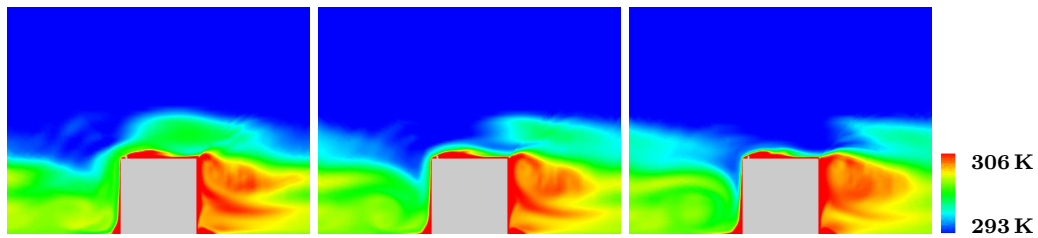
(b) Cube with vortex generator 1

(c) Cube with vortex generator 2

Figure 5.9: Distribution of the instantaneous temperature in the plane z/H=0

ure 5.9 in three different instants for each of the varied cubes. Over the cube without a vortex generator (figure 5.9a), the more steady temperature layers seem to be closer to the cube, than over the cubes with vortex generators. That leads to a better mixing of the upper colder

and the lower and warmer air in case of a cube with VG than a cube without a VG.

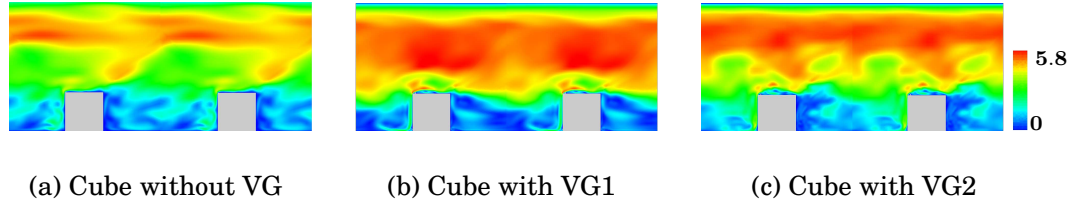Figure 5.10 shows instantaneous velocity fields around two cubes in a

| (a) Cube without VG | (b) Cube with VG1 | (c) Cube with VG2 |

Figure 5.10: The plane z/H=0 colored with the velocity magnitude in one instant. $[m/s]$

line for each case. The wake of one cube affects the conditions of the next cube. If the wake of the cube is more turbulent, then the heat transfer of the next cube can be enhanced. The vortices that are shed from the cubes with vortex generators are more turbulent than the vortices in the wake of the smooth cube. Hence, the vortices behind the cubes with vortex generators involve colder air from above in the cooling of the following cube in line.

The influence of the vortex generators on the instantaneous flow is also studied by means of several movies displaying instantaneous flow properties around the varied cubes. These movies show that the frequency of vortex shedding behind the VGs is higher than the dominant vortex shedding in the flow. More about these movies can be found in the Appendix A.

5.4 Heat Transfer

The heat transfer between the cube and the air is changing due to the existence of vortex generators.

The temperatures around the cubes and at the cubes' surfaces are showing a change due to the different flow structures with vortex generators than without. Figure 5.11 shows the contours of the time-averaged temperatures at the plane $y/H = 0.5$ for the different cubes.
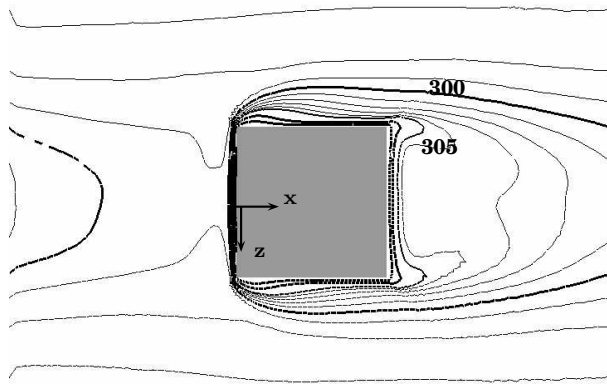
(a) Cube without vortex generator
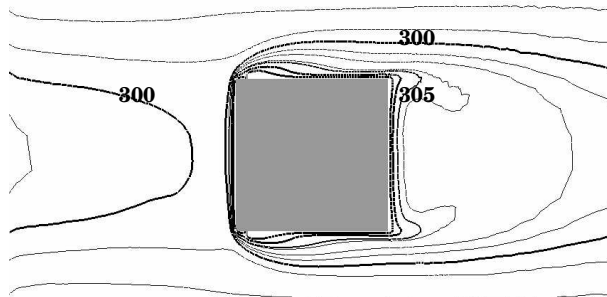
(b) Cube with vortex generator 1
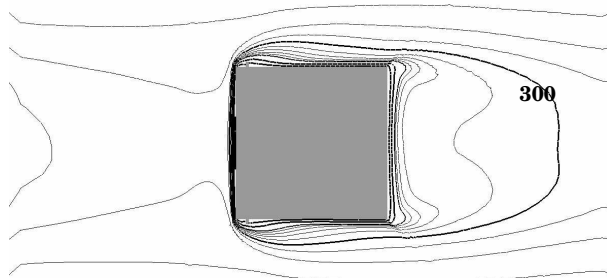
(c) Cube with vortex generator 2

Figure 5.11: The contours of the time-averaged temperature at the plane $y/H = 0.5$. [K]

45

In figure 5.12 some temperature profiles in the vertical zy-plane z/H=0 close to the surface of the cube are displayed. The black lines represent the profiles of the cube without vortex generator and the dashed grey lines are the profiles of the cube with vortex generator 1, while the light grey dash-dot lines are representing the profiles of the cube with vortex generator 2.
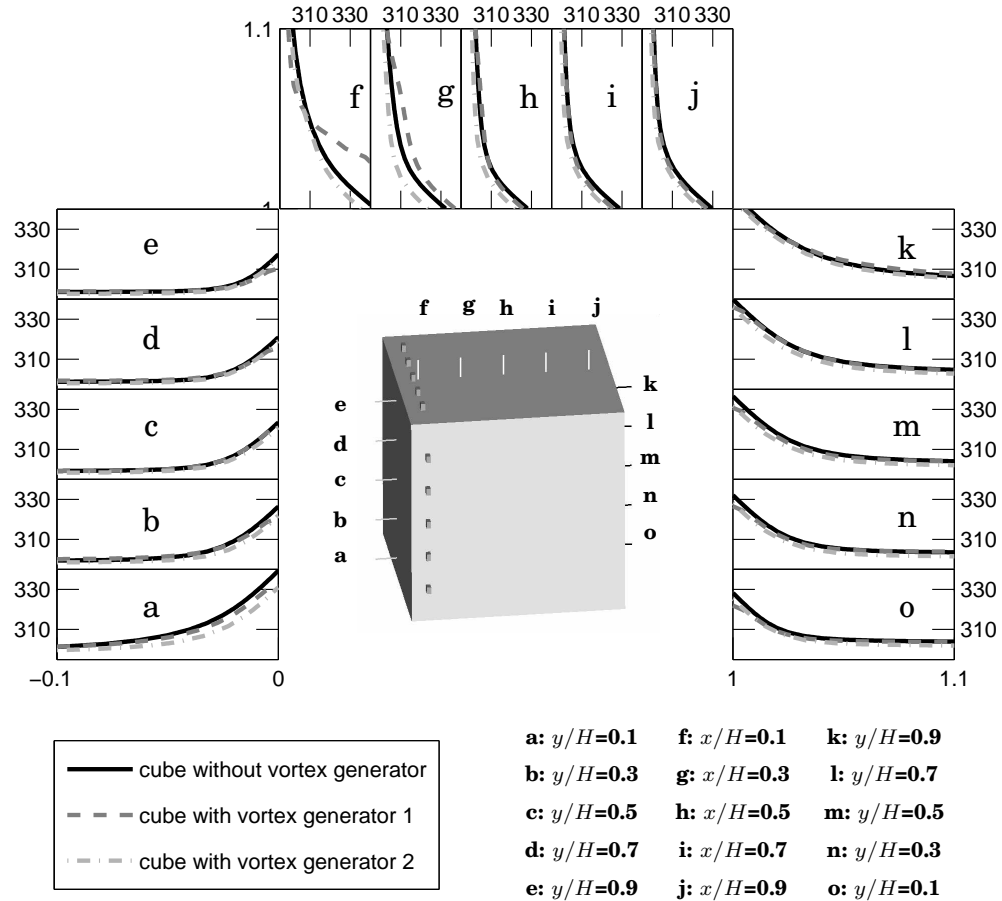

a: y/H=0.1	**f:** x/H=0.1	**k:** y/H=0.9
b: y/H=0.3	**g:** x/H=0.3	**l:** y/H=0.7
c: y/H=0.5	**h:** x/H=0.5	**m:** y/H=0.5
d: y/H=0.7	**i:** x/H=0.7	**n:** y/H=0.3
e: y/H=0.9	**j:** x/H=0.9	**o:** y/H=0.1

Figure 5.12: Temperature boundary layer profiles in the vertical xy-plane z/H=0.

As expected, high temperatures at the surface of the cube are found, where the flow is separated from the faces or where the flow circulates. Figure 5.7 of the time-averaged streamlines at the $xy-$plane at z/H=0 shows that there is a circulation region in front of the cube close to the grounded edge and also behind the cube close to the upper edge. A separation region can be found at the at the top-side face close to the

windward edge of the cube. All these locations at the surface of the cube are characterised with high temperatures, figure 5.12 (a), (f) and (k).

One can also see in figure 5.12, that the temperature of the air around the cube with VG2 is nearly always the lowest. The temperature around the cube with VG1 is in most of the pictures lower than the temperature around the cube without VG, but it is very high in picture (f) and (g) close to the cube. The VG1 leads to high temperature spots behind the rib by trapping the heat inside the circulating flow, and hence a bad heat transfer in that area can be expected.

At the distance of $0.1/H$ to the cube's surface, all the three lines seem to be very close in every picture. Thus the gradient of the temperature of the smooth cube is always higher than the gradient of the cube with VG2.

The temperature of the surface of the cube T and the inlet bulk temperature T_{bi} are used to get to know the local heat transfer coefficient h as:

$$h = \frac{\dot{Q}/A}{(T - T_{bi})}. \tag{5.1}$$

Here $\dot{Q}$ is the heat dissipated by the cube and A is the cubes surface. Figure 5.14 shows the time-averaged local heat transfer coefficient h at each face of the different cubes.

As expected, the heat transfer coefficient h is low, where the flow is separated and high, where the flow is attached to the surface. Due to the figure 5.4 of the time-averaged streamlines, at the top faces of the cubes the flow separates first and later on it reattaches to the surface. Hence the heat transfer coefficient h is low on the top-side face close to the windward edge and high close to the leeward edge.

The influence of the vortex generators is also shown in figure 5.13 by means of the quantitative representation of the mean heat transfer coefficient at three different cross sections of the cube. That figure presents a higher heat transfer coefficient at the cubes with VGs except close behind the VG1. Here the heat transfer coefficient is found to be very low.

47
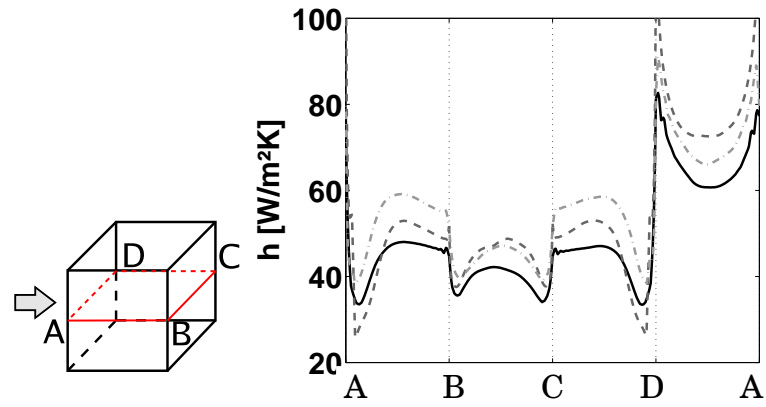
(a) The path ABCDA in the horizontal xz-plane at y/H=0.5.
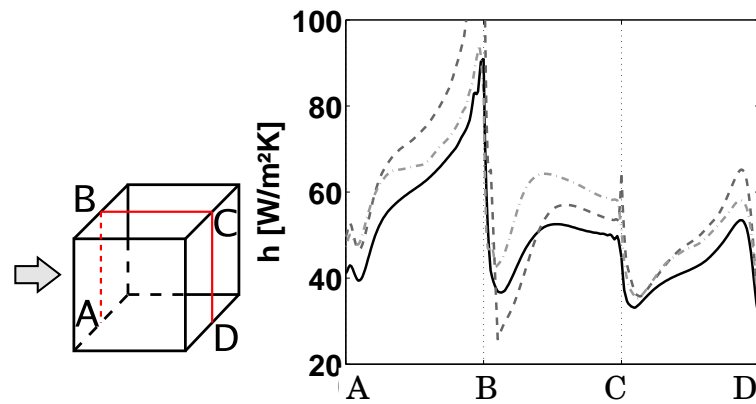
(b) The path ABCD in the vertical xy-plane at z/H=0.
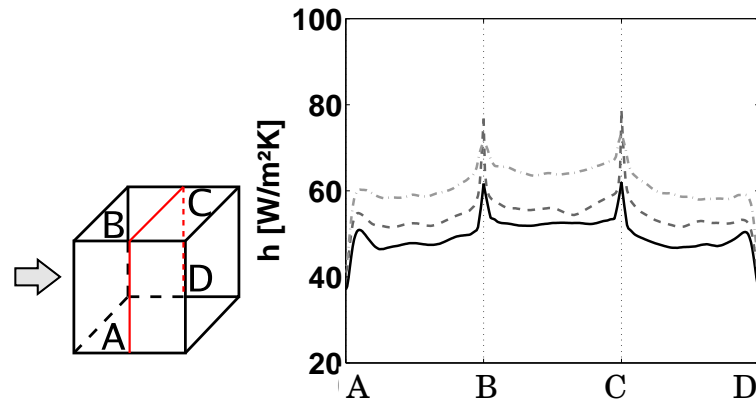
(c) The path ABCD in the vertical yz-plane at x/H=0.5.

Figure 5.13: Distribution of the time-averaged local heat transfer coefficient along different paths. Solid line: Smooth cube; dashed line: Cube with VG1; dash-dot line: Cube with VG2.

(a) Cube without vortex generator

(b) Cube with vortex generator 1

(c) Cube with vortex generator 2
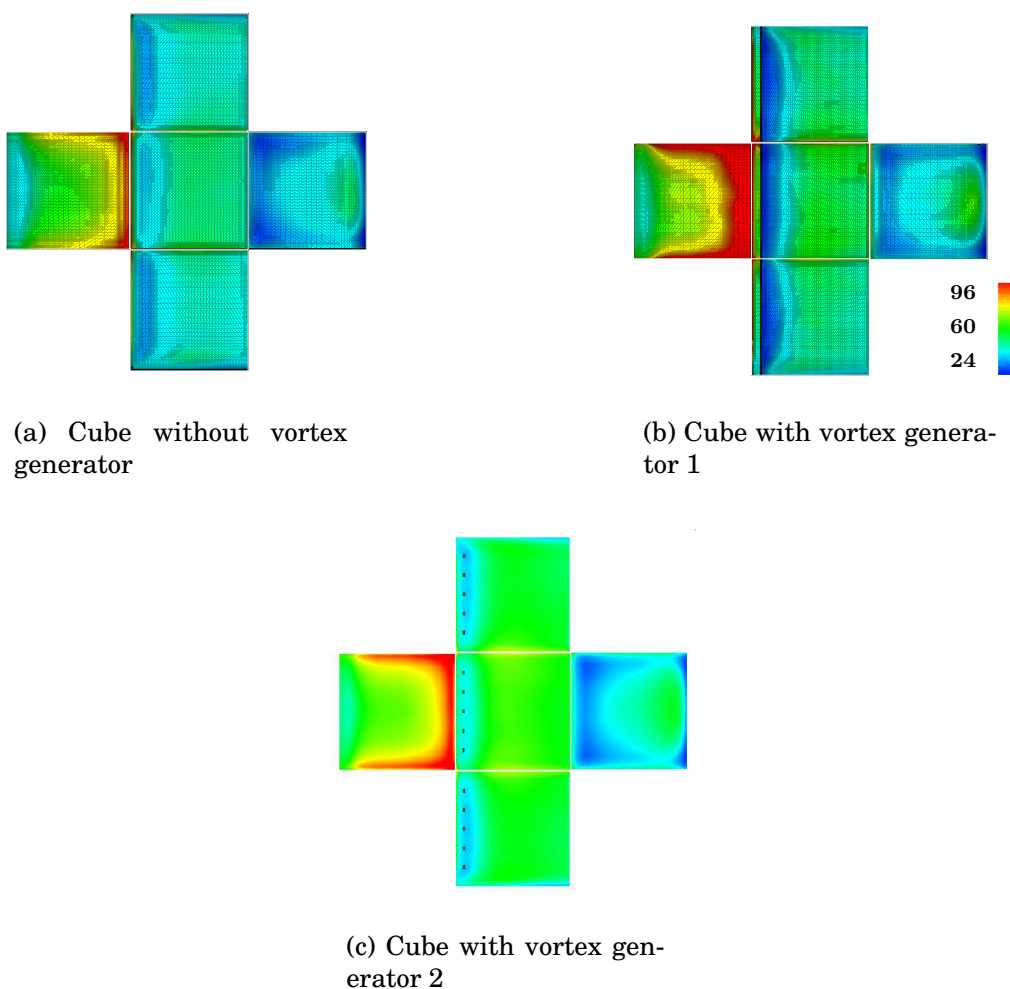
Figure 5.14: The faces of the cubes, colored by the time-averaged heat transfer coefficient h. [W/m^2K]

Further more, the mean heat transfer coefficient is calculated at each face of the varied cubes as an average over the surface as the following:

$$h = \frac{1}{A} \int\limits_{(A)} \frac{\dot{Q}/A}{(T - T_\infty)} dA \; , \qquad (5.2)$$

Where $\dot{Q}$ is the constant heat loss of the cube and A is the area of the face of the cube.

Globally, the mean heat transfer coefficient of the cube without a vortex generator is 48.92 $\frac{W}{m^2K}$. It increases by attaching vortex generators at

49

the surface to a value of 55.62 $\frac{W}{m^2K}$ with vortex generator 1 and a value of 57.07 $\frac{W}{m^2K}$ with vortex generator 2. That implies a change of 13.7% of the heat transfer coefficient h between the smooth cube and the cube with VG1. The percentage of increase of h between the different vortex generators VG1 and VG2 is not very big, but the most intensification of heat transfer can be found between the cube without a VG and the cube with VG2. The percentage of increasing h is about 16.66% here.

Table 5.3 lists all the values of the mean heat transfer at each face of the cube and table 5.4 includes the percentage of increase of h between the varied cubes for each face and the total cube.

Cube face	Cube without VG	Cube with VG1	Cube with VG2
Front	65.96	82.87	73.30
Top	49.75	52.93	59.75
Lee-side	38.79	44.19	43.03
Lateral-sides	45.05	49.06	54.69
Total cube	48.92	55.62	57.07

Table 5.3: The mean heat transfer coefficient h at each face of the cube [$\frac{W}{m^2K}$]

Cube face	without VG to VG1	VG1 to VG2	without VG to VG2
Front	25.64	-11.55	11.13
Top	6.39	12.88	20.10
Lee-side	13.92	-2.63	10.93
Lateral-sides	8.90	11.48	21.40
Total cube	13.70	2.61	16.66

Table 5.4: The percentage of increase of h

Although the increase of h between the cube with VG1 and VG2 is only 2.61%, the VG2 might still be prefered, since the heat transfer for that cube is more consistent over all faces of the cube. At the cube with VG1, there are local spots with a very low heat transfer coefficient behind the rib, as one may see in figure 5.14 (b). Hence, the temperature at the faces of this cube differs more and there are parts with much higher temperature as the mean temperature at the surface of the cube.

To compare the temperature variation at the faces of the three cubes, it is useful to calculate the root mean square deviation σ_T:

$$\sigma_T = \sqrt{\frac{1}{A} \int\limits_{(A)} \left(\overline{T} - T(\vec{x})\right)^2 dA} \ .$$

(5.3)

Here, A is the area of the faces of the cube, $\overline{T}$ is the mean temperature averaged over this area and T is the local time-averaged temperature.

The standard deviation σ_T for the cube without a VG is 8.56 K, for the cube with VG1 it is 10.90 K and for the cube with VG2 it is 7.55 K. It is obvious, that the temperature of the cube with VG2 is distributed the most even and hence this cube is most resistant against local overheating.

Chapter 6

Conclusions

Large-eddy simulation was successfully used to investigate the influence of attaching different vortex generators on the surface of wall-mounted heated cubes on the local heat transfer coefficient.

Meshes consisting of C- and O-grids topologies were used in the simulations which reduced the number of cells needed for a good spatial resolution considerably. LES results for the flow and the temperature distributions were obtained for surface-mounted smooth cubes and cubes with two different vortex generators, the first rib-shaped and the second composed of small cuboids. A very fine and a coarser mesh around the cube with the second vortex generator were made to ensure that the results are independent of the mesh resolution. The LES results were found to be in a good agreement with the experimental data for the case without vortex generator for which the experimental data exists.

The relation between the flow structures around the cube and the temperature distribution is explained in this thesis. The streamwise front face of the cube was found to have a high heat transfer coefficient especially where the flow moves upwards carrying the heat from the face. A lower local heat transfer coefficient is reported at places where flow circulation occurs such as on the lee-side face close to the cube's edges and also at the top-side face and the lateral faces close to the windward edges where flow-separation regions can be found.

Attaching vortex generators to the top and the lateral faces of the cube turned out to shorten the distance of flow separation at these faces. Hence, the length of reattached flow increased and the local heat transfer coefficient is enhanced especially at these locations.

It was found that the vortex generators altered the boundary layer on the surface of the cube. As a result, vortices are shed from the wake of the vortex generator at a higher frequency than the dominant vortex shedding in the flow. These vortices are characterized by higher unsteadiness and more complex structures than the boundary layer vortices without the vortex generator. Globally these vortices enhanced the mixing of heat in the boundary layer which led to high mean heat transfer coefficients at the cubes with vortex generators.

The present investigation showed that the increase of the heat transfer coefficient is considerable. Local high temperature spots were found in the circulation region behind the rib-shaped vortex generator (VG1), but the temperature distribution at the cube with the second vortex generator (VG2) was found to be very even, actually more evenly distributed than at the smooth cube. Hence, the overheating problem behind the VG1 disappeared in case of VG2. There was an increase of the mean heat transfer coefficient of about 13.7% having a rib-shaped vortex generator at the cube's surfaces instead of a smooth cube. There was an increase in the time-averaged heat transfer coefficient of 16.66% for the cube with vortex generator 2.

Bibliography

[1] S. Krajnović and L. Davidson. Flow around a three-dimensional bluff body. *9th International Symposium on Flow Visualization*, 2000.

[2] E.R. Meinders and K. Hanjalić. Experimental study of the convective heat transfer from in-line and staggered configurations of two wall-mounted cubes. *International Journal of Heat and Mass Transfer*, 45:465–482, 2002.

[3] S. Krajnović and L. Davidson. Large-eddy simulation of the flow around a bluff body. *AIAA Journal*, 40(5):927–936, 2002.

[4] R. Martinuzzi and C. Tropea. The flow around surface-mounted prismatic obstacles placed in a fully developed channel flow. *ASME: Journal of fluid Engineering*, 115:85–91, 1993.

[5] A. Yakhot, H. Liu, and N. Nikitin. Turbulent flow around a wall-mounted cube: A directnext term numerical simulation. *International Journal of Heat and Fluid Flow*, 27:994–1009, 2006.

[6] H. Nakamura, T. Igarashi, and T. Tsutsui. Local heat transfer around a wall-mounted cube at 45° to flow in a turbulent boundary layer. *International Journal of Heat and Fluid Flow*, 24:807–815, 2003.

[7] E.R. Meinders and K. Hanjalić. Vortex structure and heat transfer from in-line and staggered configurations of two wall-mounted cubes. *International Journal of Heat and Mass Transfer*, 20:255–267, 1999.

[8] B.Ničeno, A.D.T. Dronkers, and K. Hanjalić. Turbulent heat transfer from a multi-layered wall-mounted cube matrix: a large eddy simulation. *International Journal of Fluid Flow*, 23:173–185, 2002.

[9] Y. Cheng, F. Lien, E. Yee, and R. Sinclair. A comparison of large-eddy simulations with a standard $k - \epsilon$ reynolds-averaged navier-stokes model for the prediction of a fully developed turbulent flow over a matrix of cubes. *Journal of Wind Engineering and Industrial Aerodynamics*, 91:1301–1328, 2003.

[10] B. Zhong and P.G. Tucker. $k-l$ based hybrid les/rans approach and its application to heat transfer simulation. *International Journal for Numerical Methods in Fluids*, 46:983–1005, 2004.

[11] Masaru Koike, Trunehisa Nagayoshi, and Naoki Hamamoto. Research on aerodynamic drag reduction by vortex generators. *Mitsubishi Motors Technical Review*, (16), 2004.

[12] Mitsubishi lancer evolution ix. *http://www.seriouswheels.com/2006/2006-Mitsubishi-Lancer-Evolution-IX-Vortex-Generator-1024x768.htm*, 2006.

[13] 1967 model cessna 182k in flight showing after-market vortex generators on the wing leading edge. *http://www.answers.com/topic/vortex-generator*, 2006.

[14] Herbert Oertel jr. and Martin Boehle. *Stroemungsmechanik*. Vieweg, 3nd edition, 2004. ISBN 3-528-23893-3.

[15] Herbert Oertel jr. and Eckart Laurien. *Numerische Stroemungsmechanik*. Vieweg, 2nd edition, 2003. ISBN 3-528-03936-1.

[16] Stephen B. Pope. *Turbulent Flows*. Campridge University Press, 2nd edition, 2001. ISBN 0-521-59886-9.

[17] David C. Wilcox. *Turbulence Modeling for CFD*. DCW Industries, 2nd edition, 2002. ISBN 1-928729-10-X.

[18] P.A. Davidson. *Turbulence*. Oxford University Press, 2nd edition, 2004. ISBN 0-19-852949-X.

[19] Fluent6.2 documentation. 2005.

[20] Incropera, DeWitt, Bergman, and Lavine. *Fundamentals of Heat and Mass Transfer*. John Wiley and Sons Inc, 6nd edition, 2006. ISBN 0-471-45728-0.

[21] J. Laufer. Investigation of turbulent flow in a two dimensional channel. *N.A.C.A. Report*, 1053, 1951.

[22] Jan Eriksson Rolf I. Karlsson Lennart Lfdahl Martin Wosnik William K. George, Hans Abrahamsson. A similarity theory for the turbulent plane wall jet without external stream. *J. Fluid Mech.*, 425:367–411, 2000.

Appendix A

In addition, for the analysis of the influence of the different vortex generators on the instantaneous flow, several movies are made, consisting of 500 time steps. The movies can be found in Appendix B.

The velocity magnitude and the temperature distribution around the smooth cube and the cubes with VG1 and VG2 in the vertical plane z/H=0 are shown in the movies 5.1, 5.2 and 5.3, respectively.
Generally, high temperatures close to the cube can be found especially at places with a low velocity magnitude at the same time. While flow with high velocity carries the heat away from the cubes.
The temperatures over the cube without a vortex generator seem to be more steady in the upper streams than over the cubes with vortex generators. That leads to a better mixing of the upper colder and the lower and warmer air in case of a cube with VG than a cube without a VG. Close to the surface of the cube, there are more turbulent structures generated by the vortex generators than without a VG.

The movies 5.4 and 5.5 show a matrix of four and two cubes, respectively, without vortex generators and its velocity field around it in the horizontal plane y/H=0.4. The wake of one cube affects the conditions of the next cube. If the wake of the cube is more turbulent, then the heat transfer of the next cube can be enhanced. The velocity magnitudes around two cubes with VG1 can be beheld in the vertical plane z/H=0 in the movie 5.6. One may notice, that the vortices are shed from the wake of the vortex generators at a higher frequency than the dominant vortex shedding in the flow. These vortices are very unsteady and they consist of complex structures, so they involve colder air from above in the cooling of the cube.

The sequences of the velocity magnitude and the temperature around the cube without a vortex generator and around the cube with VG2 in the horizontal plane y/H=0.5 are displayed in the movies 5.7 and 5.8a). In the movie 5.8b) one can see the same, but closer to the cube

with VG2. It turns out, that the flow in the boundary layer around the cubes with vortex generators is more turbulent and unsteady than without VG.

The movies 5.9, 5.10 and 5.11 show the vertical velocity component, the y-velocity, in the horizontal plane y/H=0.4 around the smooth cube and the cubes with vortex generators. One can see much more velocity changes at the lateral sides behind the vortex generators than at the smooth cube, comparing the distance of the contour-lines close to the cube with those of the bulk flow.

The vortex generators lead to a high frequency of vortex shedding and these vortices are very unsteady and turbulent.